PEOPLE'S DEMOCRATIC REPUBLIC OF ALGERIA
MINISTRY OF HIGHER EDUCATION AND SCIENTIFIC RESEARCH
KASDI MERBAH UNIVERSITY -OUARGLA
Faculty of Mathematics and Matter Sciences
Department of Physics

Academic Master Memory

Field: Sciences of matter

Specialty: Meteorological physics

Theme

Study and analysis of Atmospheric Stability Indices in a Desert Environment

Prepared by the student: BENATALLAH Lina

Publicly defended on 18/06/2026

Before a jury composed of:

Mr. Ben Belgacem Khelfallah	MCA.	Ouargla. Univ	President
Mr. HEBBAL Belkhir	MCB.	Ouargla. Univ	Examiner
Mr. KHODJA Sebti	MCA.	Ouargla. Univ	Supervisor
Mr. FEKIH Abdellali	MCA.	Ouargla. Univ	Co-Supervisor

Academic year : 2025 / 2026

Thanks

First of all, I would like to thank Almighty Allah who gave me the strength and courage to carry out this modest work.

A big thank to my supervisor Mr. KHODJA Sebti, lecturer at the University of Ouargla who agreed to supervise me and for encouraging me in this study. He was available all the time, meeting all my expectations and questions, thank you for the trust he placed in me. I thank him very sincerely. I would also like to thank my Co-supervisor Mr. FEKIH Abdellali for allowing me to benefit from this fruitful advice and to introduce me to research work.

My sincere thanks also go to Mr. Ben Belgacem Khelfallah, professor at the University of Ouargla for having accepted without hesitation to be the president of the jury and to Mr. Mr. HEBBAL Belkhir, lecturer at the University of Ouargla for having honored me with his presence in his capacity as examiner.

Thank you to all of my teachers without obligating anyone for participating in my training during the teaching course and for being available throughout the years of study.

Thank you also to all my colleagues for their exceptional support during our university training course, particularly those in the "meteorological Physics" specialty.

Dedication

I dedicate this work with deep love and gratitude to my dear parents, especially my father, Mammar, and my mother, Dalila, for their endless support, patience, encouragement, and sacrifices throughout my studies. Their love and guidance have always been my greatest strength.

To my beloved sisters, Nesrine, Rania, Hana, Ferial, and Ines, thank you for your love, motivation, and constant support.

To my dear brother Ibrahim thank you for always being there for me.

I would also like to express my sincere appreciation to all my friends and relatives whose encouragement and kindness accompanied me throughout this journey.

This achievement is dedicated to all of you with love and gratitude

الملخص

تهدف هذه الدراسة إلى تحليل الاستقرار الجوي في بيئة صحراوية . وقد تم اعتماد حالة دراسية متمثلة في حدث مطري رعدي (عاصفي) أثر على عدة ولايات من جنوب الجزائر، من بينها توقرت، غرداية، الوادي، المغير، الأغواط، ورقلة، وذلك ابتداءً من مساء يوم الجمعة 12 الى14 افريل 2024، حيث تميز هذا الحدث بأمطار محلية معتبرة ونشاط رعدي واضح.تركزت الدراسة بشكل خاص على ولايتي الأغواط وورقلة باعتبارهما مناطق ممثلة لديناميكية هذا الاضطراب الجوي، من أجل تحليل تطور الظواهر الحملية زمنياً ومكانياً. البيانات المستخدمة في هذه الدراسة مستمدة من إعادة التحليل ERA5 التابعة لـ ECMWF؛ وهي لا تمثل قياسات مباشرة، بل حقولًا جوية مُعاد بناؤها من خلال استيعاب البيانات داخل نموذج عددي. وتحليل البروفيلات الرأسية للغلاف الجوي باستعمال مخطط Skew-T logP، إضافة إلى حساب مؤشرات الاستقرار الجوي مثل مؤشر الرفع(LI) ، مؤشرK ، مؤشر Totals Totals (TTI)، الطاقة الكامنة الحملية المتاحة(CAPE) ، وكبح الحمل الحراري **(**CIN**) .** دراسة حالة لتحليل الاستقرار الجوي فوق منطقتي الأغواط وورقلة، بما في ذلك معالجة البيانات لتقييم مدى دقة وفعالية هذه المؤشرات في الظروف الصحراوية. وتخلص الدراسة إلى أن مؤشرات الاستقرار الجوي تظهر تبايناً واضحاً حسب الظروف المحلية، مع إبراز بعض القيود في تطبيقها التقليدي في البيئات الجافة مقارنة بالمناطق الرطبة، مما يستدعي مزيداً من التكييف والتفسير عند استخدامها في المناطق الصحراوية.

الكلمات المفتاحية :الاستقرار الجوي – قياسات الطبقات العليا – مخططات الرصد الجوي – مؤشرات الاستقرار

ABSTRACT

This study focuses on the analysis of atmospheric stability in a desert environment, charact. A convective rainstorm event affected several wilayas in southern Algeria, including Touggourt, Ghardaïa, El Oued, El M'Ghair, Laghouat, and Ouargla. These disturbances began and gradually intensified from the afternoon of Friday, April 12, 2024,until April 14,2024, resulting in locally heavy rainfall accompanied by marked thunderstorm activity.In a second step, the analysis was more specifically focused on the wilayas of Laghouat and Ouargla, which are representative of the dynamics of this event, in order to examine in greater detail the spatio-temporal evolution of precipitation and associated convective phenomen. The present work investigates this convective precipitation event that affected the regions of Laghouat and Ouargla, located in the arid zone of southern Algeria. The main objective is to assess the behavior and relevance of the main atmospheric stability indices used in meteorology, namely the Lifted Index (LI), the K Index (KI), the Total Totals Index (TTI), the Convective Available Potential Energy (CAPE), and the Convective Inhibition (CIN). The data used in this study are derived from the ERA5 reanalysis provided by the ECMWF; they are not direct observations but atmospheric fields reconstructed through data assimilation within a numerical model, the analysis of vertical atmospheric profiles using the Skew-T log-P diagram, and the computation of stability indices from theoretical formulations. The results highlight a significant variability of the indices depending on local conditions, particularly under the influence of strong surface heating and low atmospheric moisture. They also reveal certain limitations in the classical interpretation of these indices in desert environments compared to other climatic settings.

Keywords: Atmospheric stability - Soundings measurements –Meteorological diagrams – Stability Indexes

Résumé

Cette étude porte sur l'analyse de la stabilité atmosphérique en environnement désertique. Un épisode pluvio-orageux a touché plusieurs wilayas du Sud algérien, notamment Touggourt, Ghardaïa, El Oued, El M'Ghair, Laghouat et Ouargla. Ces perturbations ont débuté et se sont progressivement intensifiées à partir de l'après-midi du vendredi 12 au 14 avril 2024, donnant lieu à des pluies parfois soutenues accompagnées d'une activité orageuse localement marquée. Dans un second temps, l'analyse s'est concentrée plus particulièrement sur les régions de Laghouat et Ouargla, zones représentatives de la dynamique de cet épisode, afin d'étudier plus finement l'évolution spatio-temporelle des précipitations et des phénomènes convectifs associés. Le présent travail s'intéresse à cet épisode pluvio-orageux ayant affecté les régions de Laghouat et Ouargla, situées en zone aride du Sud algérien. L'objectif principal est d'évaluer le comportement et la pertinence des principaux indices de stabilité atmosphérique utilisés en météorologie, notamment l'indice de soulèvement (LI), l'indice K (KI), l'indice Total Totals (TTI), l'énergie potentielle convective disponible (CAPE) et l'inhibition convective (CIN). Les données utilisées dans cette étude proviennent de la réanalyse ERA5 fournie par le ECMWF ; elles ne constituent pas des observations directes, mais des champs atmosphériques reconstruits par assimilation de données dans un modèle numérique, l'analyse des profils verticaux de l'atmosphère à l'aide du diagramme Skew-T log-P, ainsi que le calcul des indices de stabilité à partir de formulations théoriques.. Les résultats mettent en évidence une variabilité significative des indices en fonction des conditions locales, notamment sous l'effet du fort échauffement de surface et de la faible humidité de l'air. Ils montrent également certaines limites dans l'interprétation classique de ces indices en milieu désertique, comparativement à d'autres environnements climatiques

Mots-clés: Stabilité atmosphérique – Mesures de sondages – Diagrammes météorologiques – Indices de stabilité.

Table of Contents

Thanks I
Dedication II
ABSTRACT IV
Résumé V
List of Figures IX
List of Tables X
Lists of abbreviations and symbols XI
General Introduction 1
CHAPTER I: GENERAL INFORMATION ON ATMOSPHERIC STABILITY
I.1. Introduction 3
I.2. Vertical Structure of the Atmosphere 3
I.2.1. Different layers of the atmosphere 3
I.2.1.1.The troposphere 3
I.2.1.2.The stratosphere 3
I.2.1.3.The mesosphere 3
I.2.1.4.The thermosphere 4
I.3. Upper-Air Observations for Atmospheric Stability Analysis 4
I.3.1. Definition and Operation of the Radiosonde 5
I.3.2. History and Development of the Radiosonde 5
I.3.3. Principles of Radiosonde Operation and Atmospheric Measurements 6
I.4. Radiosonde Launch Procedure 7
I.4.1. Balloon Inflation 7
I.4.2. Measurement Methods 9
I.4.3 Reception and Data Processing System 10
I.5. ERA5 Reanalysis 12
I.6. Thermal Gradients 12
I.6.1. Definition of the Vertical Thermal Gradient 12
I.6.2. Environmental Lapse Rate (Γenv) 13
I.6.3. Dry Adiabatic Lapse Rate (Γ_d) 13
I.6.4. Saturated Adiabatic Lapse Rate (Γs) 14
I.6.5. Factors Influencing Thermal Gradients 14
I.6.6.Comparison of the Gradients 14

I.6.7. Role in Atmospheric Stability 14
I.7.Thermodynamic Diagrams in Meteorology 15
I.7.1.The Emagram 761 16
I.7.1.1.Orientation of Fundamental lines 19
I.7.2.The SkewT /log p 19
I.7.2.1.Orientation of the fundamental lines 20
I.8. Difference between the Skew-T logP) diagram and the Emagram 761 21
I.9. Conclusion 23

CHAPTER II: STABILITY INDICES OF THE ATMOSPHERE

II.1. Introduction 24
II.2. Stability and instability of an air particle in the atmosphere 24
II.2.1. Atmospheric stability 24
II.2.2. Atmospheric Instability 24
II.3.Shematic illustration of atmospheric stability and instability processes 24
II.3.1.Equilibrium case of unsaturated air 24
II.3.2.Equilibrium cases of saturated air 27
II.3.3. Conditional (or latent) instability of an air parcel 29
II.4. Main levels that can be reached by an adiabatically lifted air parcel 29
II.4.1. Lifting Condensation Level (LCL) 29
II.4.2. Convective Condensation Level (CCL) 30
II.4.3. Level of Free Convection (LFC) 30
II.4.4. Equilibrium Level (EL) 31
II.5. Stability indices 32
II.5.1. Showalter Index (SI) 32
II.5.2.K-Index (KI) 33
II.5.3. Lifted Index (LI) 33
II.5.4. SWEAT Index 34
II.5.5. Total Totals Index (TTI) 34
II.5.6. Convective Available Potential Energy (CAPE) 35
II.5.7.Convective Inhibition (CIN) 35

CHAPTER III: ANALYSIS OF ATMOSPHERIC STABILITY INDICES

III.1. Introduction 37
III.2. Geographical and climatological characteristics of the Laghouat and Ouargla regions 37
III.2.1.The region of Laghouat 37
III.2.2. The region of Ouargla 38

III.3. Data Sources and Methodology 39
III.4. Presentation of ERA5 reanalysis data from the ECMWF 39
III.4.1. ERA5 reanalysis data of Laghouat region.. 39
III.4.1.1. Stability indices of the Laghouat region 41
III.4.1.2. Interpretation of atmospheric stability of the Laghouat region 42
III.4.2.ERA5 reanalysis data of Ouargla region 43
III.4.2.1. Stability indices of the Ouargla region 45
III.4.2.2. Interpretation of atmospheric stability of the Ouargla region 45
III.4.3. Comparative analysis of atmospheric stability between both regions 46
III.5. Conclusion.. 48
Conclusion General 50
Bibliographic References ....

List of Figures

Figure (I.1): Thermal structure of the atmosphere 4

Figure (I.2): Global Distribution of Radiosonde Launch Site.. 6

Figure (I.3): Vaisala RS92-SGP Radio Probee... 7

Figure (I.4): Meteorological balloon inflation and preparation for radiosonde launch 9

Figure (I.5): The electronic rack for radiosonde reception..11

Figure (I.6): Emagram in rectangular coordinates 17

Figure (I.7): Emagram761 18

Figure (I.8): Skew-T diagram... 20

Figure (I.9): Emagram (left) and Skew-T logP diagram (right), showing the different graphical constructions used to represent atmospheric thermodynamic profiles... 22

Figure (II.1): Stable Equilibrium.. 25

Figure (II.2): Unstable equilibrium 26

Figure (II.3): Neutral equilibrium 27

Figure (II.4): Stable equilibrium 28

Figure (II.5): Unstable equilibrium 28

Figure (II.6): Neutral equilibrium 29

Figure (II.7): Illustration of the Lifted Condensation Level (LCL) on a Skew-T Diagram…....... 30

Figure (II.8): Determination of the Level of Free Convection (LFC) on a Skew-T Diagram 31

Figure (II.9): Determination of the Equilibrium Level (EL) on a Skew-T Diagram 32

Figure(III.1):Geographical location of the Laghouat region in Algeria... 37

Figure (III.2):Geographical location of the Ouargla region in Algeria 38

Figures (III.3):(a,b),(c,d),(e, f) Days of 12,13,14 /April 2024 for 00h and 12h UT respectively ... 41

Figures(III.4): (g,h),(i,j),(k, l) Days of 12,13,14 /April 2024 for 00h and 12h UT respectively..... 44

List of Tables

TABLE (III.1): Stability Indices for 12 April 2024 41
TABLE (III.2): Stability Indices for 13 April 2024 41
TABLE (III.3): Instability Indices for 14 April 2024 42
TABLE (III.4):Stability Indices for 12 April 2024 45
TABLE (III.5): Stability Indices for 13 April 2024 45
TABLE (III.6): Stability Indices for 14 April 2024 45

Lists of abbreviations and symbols

CAPE: Convective Available Potential Energy

CAF: Automatic Frequency

CIN (or CINE): Convective Inhibition Energy *(form standard: CIN)*

(ECMWF): European Centre for Medium-Range Weather Forecasts

GPS: Global Positioning System

KI: K Index

LCL: Lifting Condensation Level

CCL: Convective Condensation Level

LFC: Level of Free Convection

EL: Equilibrium Level

WMO: World Meteorological Organization

ONM: National Office of Meteorology

SPI: Standardized Precipitation Index

TTI (or TT): Total Totals Index

SWEAT: Severe Weather Threat Index

PW: Precipitable water

FL: Freezing Level

GENERAL INTRODUCTION

General Introduction

Meteorology plays a fundamental role in understanding and predicting atmospheric processes that directly influence human activities, natural ecosystems, and socio-economic systems. By analyzing key atmospheric variables such as temperature, pressure, humidity, and wind, it provides essential tools for weather forecasting, climate monitoring, and risk assessment. These applications are particularly crucial in regions exposed to extreme climatic conditions.

Desert environments constitute a challenging field of study due to their distinctive atmospheric characteristics, including intense solar radiation, strong surface heating, low moisture content, and large diurnal temperature variations. These factors strongly influence atmospheric stability and the development of convective phenomena, thereby increasing the complexity of weather prediction.

A convective rainstorm event was observed in southern Algeria, affecting several wilayas including Touggourt, Ghardaïa, El Oued, El M'Ghair, Laghouat, and Ouargla. These disturbances began and gradually intensified from the afternoon of Friday, April 12 to April 14, 2024, leading to episodes of locally heavy rainfall accompanied by significant thunderstorm activity. In a subsequent step, the analysis was more specifically focused on the regions of Laghouat and Ouargla, which are representative of the dynamics of this event, in order to examine in greater detail the spatio-temporal evolution of precipitation and associated convective processes.

The present work investigates this convective precipitation event that affected the regions of Laghouat and Ouargla, located in the arid zone of southern Algeria.

In this context, the study focuses on the analysis of atmospheric stability in an arid environment, using Laghouat and Ouargla as case study regions. This area is representative of Saharan climatic conditions and is characterized by strong thermal contrasts and persistently dry atmospheric conditions.

The main objective of this work is to assess the behavior, performance, and reliability of the principal atmospheric stability indices, namely, Lifted Index (LI), K Index (KI), Total Totals Index (TTI), Convective Available Potential Energy (CAPE), and Convective Inhibition (CIN), in diagnosing atmospheric conditions and evaluating their effectiveness in predicting convective activity.

The methodology is based on the analysis of radiosonde data, the use of thermodynamic diagrams such as the Skew-T log-P, and the computation of stability indices from theoretical formulations.

The manuscript is organized into three chapters:

The first chapter presents the theoretical background, including atmospheric structure, thermal gradients as well as thermodynamic diagrams, and fundamental concepts of stability.

The second chapter presents the study of atmospheric stability through the displacement of an air parcel in the vertical structure of the atmosphere. It begins by describing the air parcel motion under adiabatic conditions. The different atmospheric levels that can be reached by an air parcel are then introduced such as the lifting condensation level (LCL), the level of free convection (LFC), and the equilibrium level (EL), which are essential for understanding convective development. It details also the main atmospheric stability indices used in this study, including the Lifted Index (LI), K Index (KI), Total Totals Index (TTI), Convective Available Potential Energy (CAPE), and Convective Inhibition (CIN).These theoretical elements form the basis for interpreting thermodynamic diagrams such as the Skew-T log-P and for assessing atmospheric conditions in both observational and analytical contexts.

The third and last chapter provides a case study analysis of atmospheric stability over the regions of Laghouat and Ouargla, including data processing, index computation, and discussion of the results.

The work concludes with a synthesis of the main findings, highlighting the limitations and applicability of stability indices in arid environments, along with perspectives for future research.

CHAPTER I:

GENERAL INFORMATION ON ATMOSPHERIC STABILITY

I.1. Introduction

The vertical structure of the atmosphere describes how important physical properties of air such as temperature, pressure, and chemical composition change with altitude. This stratified organization is essential for understanding a wide range of meteorological and climatic processes, including cloud formation, energy exchanges, and atmospheric circulation.

In this context, atmospheric pressure decreases rapidly with height, following an approximately exponential law, due to the progressive reduction of the air mass above a given level. Similarly, temperature does not vary uniformly with altitude; its complex vertical profile leads to the identification.

I.2. Vertical Structure of the Atmosphere

I.2.1. Different layers of the atmosphere

The atmosphere is needed for life on Earth [1]. In addition, the stratification of the atmosphere is mainly based on three parameters:

- Temperature, which distinguishes the different layers through its vertical variations.
- Pressure, which decreases exponentially with altitude.
- chemical composition, which varies particularly in the upper layers and which are:

I.2.1.1.The troposphere

The troposphere is the part of Earth's atmosphere closest to the ground, stretching about 7–16 km high. Its upper edge varies with climate, reaching 13–16 km at the equator but just 7–8 km at the poles. Temperatures in this layer drop as you go higher. The troposphere holds most of the atmosphere's mass (80-90%) and almost all of its water vapor. It's where we see, weather happen, like clouds and rain. Air also moves around in this layer, both side to side as wind and up and down because of heat [1].

I.2.1.2.The stratosphere

In the stratosphere, the temperature goes up as you go higher, getting as warm as 0°C. This layer spans from about 8–15 km to 50 km above the ground and holds around 90% of the ozone [1].

I.2.1.3.The mesosphere

In the mesosphere, temperatures drop as altitude increases, reaching about -80°C at 50 to 80 km above the Earth. This layer acts as a transition between Earth and space. Most meteoroids and satellites burn up here due to friction with air particles, preventing them from reaching the ground. Spacecraft like the Soyuz require special shielding to survive this layerwhich slows them for a safe landin [1].

I.2.1.4.The thermosphere

The thermosphere, located just below the exosphere, is a layer where temperature increases with altitude, ranging from 80 to 350–800 km. In contrast to lower layers, the air composition in this layer (and the exosphere) is not uniform because air mixing is insufficient to maintain a consistent distribution [1].

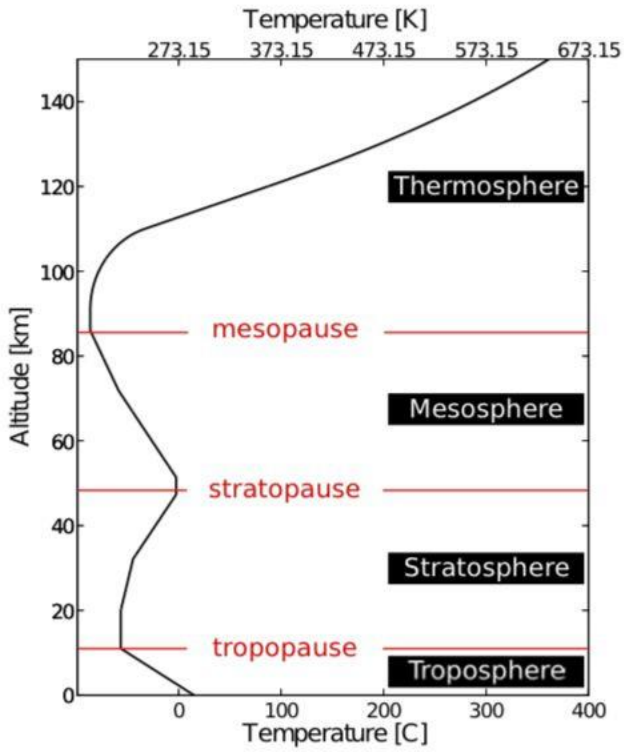

Figure (I.1): Thermal structure of the atmosphere [1].

I.3. Upper-Air Observations for Atmospheric Stability Analysis

Addressing the requirements of operational meteorology, the Global Observing System (GOS), coordinated by the World Meteorological Organization (WMO), integrates extensive upper-air observations. These observations are indispensable for calibrating and validating global numerical weather prediction models. The network employs advanced instrumentation for monitoring key atmospheric variables, including temperature, geopotential pressure, wind speed and direction, humidity, and chemical composition. National Meteorological Services

(NMS) support this framework by upholding strict adherence to WMO technical regulations across their data collection, processing, and reporting protocols. The upper-air observing network comprises several principal components:

Radiosonde Observations: These yield high-resolution vertical profiles of atmospheric conditions. Such profiles are obtained through balloon-borne instrument packages (radiosondes) that acquire in-situ thermodynamic parameters and wind data, typically extending to altitudes of approximately 30 km.

Aircraft-Based Observations: Data relayed from automated systems on commercial aircraft (AMDAR) furnish continuous meteorological information. This includes parameters like ambient temperature and wind vectors, collected throughout flight operations.

Satellite Observations: Leveraging both geostationary and polar-orbiting platforms, satellite observations complement the network by deriving vertical profiles of atmospheric properties via remote sensing techniques. This approach is crucial for achieving global coverage and maintaining data continuity [2].

I.3.1. Definition and Operation of the Radiosonde

A radiosonde, often referred to as a sonde, is an instrument designed for deployment into the atmosphere via a weather balloon. It is equipped with sensors that measure key meteorological parameters, including atmospheric pressure, temperature, and humidity world meteorological organization, 2008. Furthermore, it incorporates a radio transmitter that relays the collected data to a ground station in real time, enabling continuous monitoring of atmospheric conditions WMO,2008 [2].

I.3.2. History and Development of the Radiosonde

The development of upper-air observation techniques underwent a significant transformation with the advent of the radiosonde, an innovation designed to overcome the inherent limitations of meteorological instrumentation available in the early 20th century. Documentation indicates that Robert Bureau developed the first operational radiosonde in 1929, its initial flight occurred on January 17 of that year from the Trappes Observatory. This technological advancement merged a meteorological sensor with a short-wave radio transmitter, thereby obviating the prior requirement for physical retrieval of instrumentation. Previously, atmospheric soundings utilized 'météographes' carried aloft by kites, captive balloons, or aircraft. These earlier methodologies were frequently characterized by prohibitive costs or substantial data attrition. Bureau's specific design employed a mechanical coding system, which facilitated the transmission of temperature and pressure readings through radio signals. The methodology underlying this invention was formally presented to the French Academy of Sciences on June 10, 1929, a disclosure that firmly established its historical priority. Within the context of international meteorological collaboration, these systems underwent further refinement and deployment during the Second International Polar Year (1932-1933). Their application was particularly significant in challenging environments, including Tamanrasset and Greenland. Presently, the radiosonde retains its role as a fundamental component of the World Meteorological Organization’s (WMO) Global Observing System, delivering the crucial vertical profiles necessary for contemporary numerical weather prediction and atmospheric stability assessments [3], see figure (I.2).

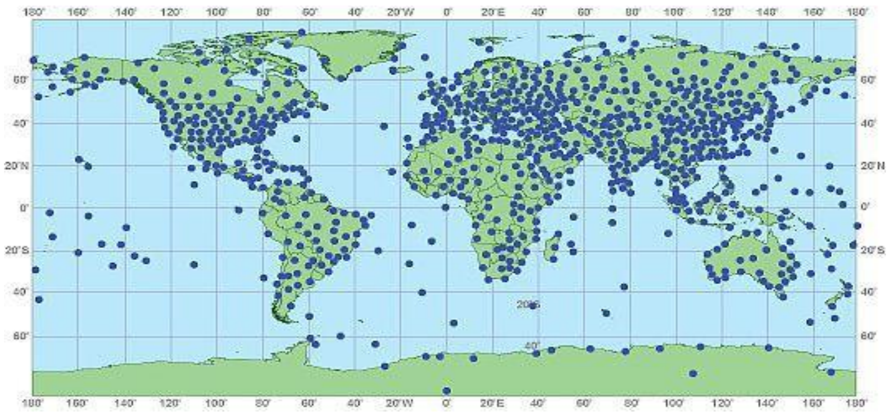

Figure (I.2): Global Distribution of Radiosonde Launch Site [4].

I.3.3. Principles of Radiosonde Operation and Atmospheric Measurements

Radiosondes are in situ atmospheric sounding instruments typically carried by helium or hydrogen-inflated latex balloons. They are intended to measure the vertical profiles of essential atmospheric variables namely pressure, temperature, and humidity from the Earth's surface up to the lower stratosphere, at approximately 30 km altitude. The measurements obtained during ascent are transmitted in real time to a ground receiving station through radio frequency communication.

Temperature and humidity data are interpreted in conjunction with measured pressure levels to establish their vertical position in the atmosphere. These primary variables enable the calculation of geopotential height, a derived vertical coordinate based on the hydrostatic balance equation, assuming constant gravitational acceleration. This approach facilitates the global comparability of atmospheric profiles while maintaining proximity to geometric altitude.

Radiosonde ascents generally include wind measurements, which are often acquired using GPS tracking systems. The balloon ascends at an average rate of about 300 m/min, resulting in a total observation period lasting roughly 1.5 to 2 hours. Data transmission occurs within internationally designated radio frequency bands, primarily between 403–406 MHz and near 1680 MHz [4].

Contemporary radiosondes are typically equipped with a GPS receiver for determining wind vectors, silicon-based pressure sensors, dual heated humidity sensors, and fast-response temperature sensors. For specific atmospheric research applications, additional sensors such as ozone analyzers or radiation detectors may be incorporated [5] see figure (I.3).

Figure (I.3): Vaisala RS92-SGP Radio Probee [6].

I.4. Radiosonde Launch Procedure

I.4.1. Balloon Inflation

- Balloon Selection and Conditioning:

The sounding procedure commences with the selection of a suitable natural rubber (latex) or synthetic balloon. The balloon's mass, typically ranging from 200g to 2000g, is determined by the anticipated burst altitude and the payload's weight. Under certain environmental conditions, such as extremely low temperatures or reduced humidity, balloons may undergo a conditioning process, involving methods like pre-heating or lubrication, to preserve elasticity and mitigate the risk of premature rupture during ascent.

- The Inflation Process (Balloon Filling):

Gas Selection: Inflation is carried out using either Hydrogen (H_2), valued for its superior lift-to-cost ratio, or Helium (He), chosen for its inherent non-flammable safety characteristics.

Operational Environment: Inflation must take place within a dedicated, well-ventilated inflation shed. This facility is designed to shield the balloon from wind-induced stresses and potential damage from sharp objects.

Contamination Prevention: In adherence to WMO standards, operators are required to wear clean cotton gloves. This practice is crucial for preventing the transfer of skin oils and acids, which could otherwise degrade the latex material and potentially lead to structural failure under the high-pressure conditions encountered in the upper atmosphere.

Lift Calculation (Free Lift): The balloon is inflated until it achieves a specified "Free Lift." This parameter is measured using calibrated counterweights, ensuring a consistent ascent rate, typically maintained between 5 and 8 m/s. This precise rate is essential for optimizing the sensor's time-constant response and for accurate calculation of wind vectors through GPS tracking.

- Rigging and Attachment:

Following inflation, the balloon's neck is secured. Subsequently, the "flight train" is attached, comprising:

The Parachute: This component is included to facilitate a controlled descent of the instrument after the balloon bursts, thereby minimizing the potential for injury or damage upon impact.

- The Unwinder (Dereler):

This is a cord, typically 20–30 meters in length, which establishes a separation between the radiosonde and the balloon. This spatial distance is critical to ensure that the sensors accurately measure the ambient atmosphere, unaffected by the wake turbulence or thermal contamination emanating from the balloon’s surface.

- Launch Execution:

The launch is scheduled to align with universal synoptic hours, specifically 00:00 and 12:00 UTC. Prior to release, a "ground check" is conducted to synchronize the radiosonde sensors with a high-precision surface weather station. Upon release, the ground station, such as a

DigiCORA system, commences real-time telemetry reception, monitoring the sonde's trajectory as it traverses the troposphere and ascends into the stratosphere [2] see figure (I.4).

Figure (I.4): Meteorological balloon inflation and preparation for radiosonde launch [5].

I.4.2. Measurement Methods

The radiosonde method involves releasing a balloon filled with a gas lighter than air, such as hydrogen or helium, into the atmosphere. The balloon typically ascends at an average vertical velocity between 4 and 8 m/s, as reported in meteorological measurement literature. A radiosonde, equipped with sensors to record pressure (P), temperature (T), humidity (H), and wind (V), is attached beneath the balloon. Data collected by these sensors are transmitted to a ground station via radio-frequency electromagnetic waves, usually near 400 MHz, which accounts for the term "radiosonde." After launch, a tethering and unwinding mechanism separates the radiosonde from the balloon, maintaining a line length of at least 25 meters to promote stable aerodynamic behavior during ascent.

To ensure a controlled descent following balloon burst, the system incorporates a parachute designed to reduce descent velocity and mitigate risks to people or property on the ground; the radiosonde typically weighs around 400 g. Although rare, there remains a potential hazard to aircraft in the event of collision with sensitive balloon components; however, such incidents are uncommon and generally considered to have negligible consequence.

Pressure, temperature, and humidity are usually measured using capacitive electronic sensors, while some systems measure temperature via thermistors. The collected signals are transformed into electrical outputs and transmitted to the ground through frequency modulation. The measurement accuracy for pressure and temperature generally aligns with operational meteorological requirements. Nevertheless, temperature readings at altitudes above approximately 10 km are subject to radiative errors, necessitating corrections from manufacturer-provided algorithms.

Humidity measurements remain the most uncertain, with discrepancies between sensor types potentially reaching 10%. Additional errors may arise when radiosondes traverse cloud layers, resulting in brief overestimation of humidity in the air above the cloud; this effect typically persists for undertwo seconds. Wind speed and direction are inferred indirectly by tracking the horizontal movement of the balloon, assuming it follows the ambient wind flow. However, traditional balloons can exhibit oscillatory and parasitic movements, which introduce additional uncertainty into wind determinations [7].

I.4.3 Reception and Data Processing System

A radiosonde reception and processing system comprises several integral components designed to facilitate the acquisition, decoding, and analysis of atmospheric data. Central to this system is a radio receiver, which may be paired with either a directional or omnidirectional antenna to capture transmitted signals effectively. Subsequently, the collected signals undergo decoding procedures that extract meteorological variables, including pressure, temperature, and humidity [5].

The system incorporates a processing unit tasked with generating standardized meteorological messages, including TEMP and PILOT reports, in accordance with World Meteorological Organization specifications. Wind measurements are acquired through tracking systems such as radio-theodolites or radar-based methods. The raw transmitted data undergo filtering, compression, and real-time visualization via specialized software, which facilitates operator oversight and system monitoring throughout the sounding procedure [5].

Data acquisition operates in a fully automated manner, with the receiver employing an automatic frequency control mechanism to compensate for frequency drift. Balloon burst detection is achieved by monitoring pressure variations or, alternatively, through altitude loss determined by GPS signals. Typically, measurements cease following the balloon burst, as the descent phase is generally deemed less relevant for atmospheric profiling.

Key measurements concentrate on the troposphere, often below altitudes of 12 to 13 km. In upper-air observations, the 100 hPa pressure level located at approximately 16,000 meters is frequently adopted as a reference point.

A standard VAISALA monitoring station comprises computer systems used for data visualization and the preliminary calibration of the radiosonde prior to flight. The reception and decoding units are combined with the radio communication equipment, and supplementary tracking systems can provide support during flight operations. The radiosonde undergoes calibration and preparation on a specialized test bench before launch, as referenced eu website, [5] see figure (I.5).

Figure (I.5): The electronic rack for radiosonde reception [5].

I.5. ERA5 Reanalysis

ERA5 reanalysis is a global dataset developed by the European Centre for Medium-Range Weather Forecasts. The acronym ERA stands for ECMWF Renalysis, while “5” indicates that it is the fifth-generation reanalysis product, which provides improved accuracy and consistency compared to previous versions.

ERA5 combines a wide range of meteorological observations, including radiosonde data, satellites, aircraft measurements, ground-based stations, in-situ observations, and ocean buoys, with a numerical weather prediction model. Through data assimilation techniques, it reconstructs a physically consistent representation of the global atmosphere.

In the context of thermodynamic analysis, such as Skew-T log-P diagrams, ERA5 allows the reconstruction of vertical profiles of temperature and dew point temperature at different pressure levels. These profiles are then used to compute atmospheric stability indices such as CAPE, CIN, and LI.

However, it is important to note that radiosonde data represent direct in-situ measurements of the atmosphere, while ERA5 provides model-based reanalysed atmospheric fields. ERA5 therefore does not correspond to a single direct observation, but rather to an optimized estimate of the atmospheric state.

Despite this difference, ERA5 is a very powerful tool, especially in regions where direct observations are sparse or irregular, such as desert environments. It enables consistent atmospheric and climatological analyses over long time periods[8].

I.6. Thermal Gradients

Thermal gradients describe the rate of change of temperature with altitude in the atmosphere. They play a fundamental role in atmospheric thermodynamics, as they determine the vertical stability of air masses and influence the development of convection. In meteorology, the comparison between the environmental thermal gradient and the adiabatic gradients (dry and saturated) allows us to assess whether an air parcel will rise, sink, or remain in equilibrium. Therefore, thermal gradients are essential for understanding cloud formation, atmospheric instability, and the initiation of weather phenomena such as storms [9].

I.6.1. Definition of the Vertical Thermal Gradient

The vertical thermal gradient describes the variation of air temperature with altitude in the atmosphere [9]. It is mathematically expressed as:

$$\Gamma = -\frac{dT}{dz} \qquad \textbf{(I.1)}$$

Where:

T is the air temperature (K or °C).

Z is the altitude (m).

Γ is the lapse rate ($K\cdot m^{1}$ or $K\cdot km^{1}$).

A positive value of Γ indicates that temperature decreases with height [10].

I.6.2. Environmental Lapse Rate (Γenv)

The environmental lapse rate represents the actual observed temperature decrease with altitude at a given time and location [9]. It is obtained from radiosonde measurements [2].

$$\Gamma_{env} = -\frac{dT_{env}}{dz} \qquad \textbf{(I.2)}$$

It is highly variable and depends on atmospheric conditions such as [10] [11]:

Time of day

Weather systems

Cloud cover

Surface heating

Typical average value: **6.5 $K\cdot km^{1}$**

I.6.3. Dry Adiabatic Lapse Rate (Γ_d)

The dry adiabatic lapse rate describes the temperature change of an unsaturated air parcel that moves vertically without exchanging heat with its surroundings [9].

From thermodynamics [9] [12]:

$$\Gamma = \frac{g}{C_P} \qquad \textbf{(I.3)}$$

Where:

g = gravitational acceleration ($9.81\ m\cdot s^{-2}$)

C_P = specific heat of air at constant pressure ($\sim 1004\ J\cdot kg^{-1}\cdot K^{-1}$)

Numerical value: $\mathbf{\Gamma_d \approx 9.8\ K\backslash km^{-1}}$

I.6.4. Saturated Adiabatic Lapse Rate (Γs)

The saturated adiabatic lapse rate applies to a moist (saturated) air parcel. During ascent, water vapor condenses and releases latent heat, which slows the cooling process. neral expression [12]:

$$\boldsymbol{\Gamma_s = \frac{g}{C_p} \cdot \frac{1+\frac{L_v \cdot q_s}{R_d T}}{1+\frac{L_v^2 \cdot q_s}{C_p R_v T^2}}} \qquad \textbf{(I.4)}$$

Where:

Lv = latent heat of vaporization

qs = saturation mixing ratio

Rd, Rv = gas constants for dry air and water vapor

T = temperature

Typical range:

4 to 7 K·km⁻¹ (depends strongly on temperature and humidity)

I.6.5. Factors Influencing Thermal Gradients

Thermal gradients depend on several physical processes [10] [11]:

- Air humidity: increases latent heat release → reduces Γs.
- Atmospheric pressure: affects air density and expansion.
- Radiative exchanges: solar heating and infrared cooling.
- Vertical motion: convection and subsidence.
- Cloud processes: condensation/evaporation effects

I.6.6.Comparison of the Gradients

The three main lapse rates satisfy the following relationship [9]:

Γs < Γenv < Γd

- Dry adiabatic lapse rate is the largest (fast cooling).
- Saturated lapse rate is the smallest (slow cooling due to latent heat).
- Environmental lapse rate varies in time and space.

I.6.7. Role in Atmospheric Stability

Atmospheric stability is determined by comparing the environmental lapse rate with adiabatic lapse rates [9][10]:

- Stability conditions:

- **Stable atmosphere:**

  $\Gamma env < \Gamma s$

  air parcels resist vertical motion

- **Unstable atmosphere**:

  $\Gamma env > \Gamma d$

  strong convection and vertical mixing

- **Conditionally unstable atmosphere**:

  $\Gamma s < \Gamma env$

  stability depends on moisture content

I.7.Thermodynamic Diagrams in Meteorology

Thermodynamic diagrams serve as prevalent tools in meteorology, offering a graphical depiction of numerous atmospheric transformations that air parcels may undergo, including isobaric, isothermal, and pseudo-adiabatic processes. While contemporary computational approaches enable the numerical analysis of these transformations, thermodynamic diagrams retain their crucial role in comprehending the vertical structure of the atmosphere. Furthermore, they facilitate the elucidation of how this structure relates to cloud formation and the progression of processes leading to precipitation [12].

An ideal thermodynamic diagram is generally expected to fulfill four key properties:

a) The area enclosed by the curve representing any cyclic process should be proportional to the energy change or the work performed.

b) As many lines as possible representing fundamental transformation sought to be straight lines.

c) The angle between isotherms and dry adiabats should be maximized.

d) In the lower atmosphere, dry adiabats should form a substantial angle with saturation adiabats.

One might initially consider employing a (P, V) or (P, α) diagram. Indeed, the elementary work performed by a unit mass of gas is defined as:

$$\boldsymbol{dW = -P\, d\alpha} \qquad \textbf{(I.5)}$$

The work executed during a cycle (or closed transformation) is given by:

$$\boldsymbol{W = -\int P\,d\alpha = \int Y\,dX} \quad \textbf{(I.6)}$$

Where X and Y are coordinates proportional to α and P, respectively. Consequently, in a (P, α) diagram, the work is proportional to the area enclosed by the closed curve, thereby satisfying property (a). However, given that variables such as V or α are not directly measurable, meteorological practice often prioritizes the use of pressure (P) and temperature (T), as these correspond to directly observable physical quantities. Nevertheless, these variables cannot be arbitrarily employed if the area is to maintain its proportionality to the work [12].

Let X and Y denote the abscissa and ordinate of a coordinate system, both being functions of meteorological variables. For the enclosed area to accurately represent the work in a cyclic transformation, the following condition must be met

$$\boldsymbol{-\int P\,d\alpha = \int Y\,dX} \quad \textbf{(I.7)}$$

Which implies:

$$\boldsymbol{\int (P\,d\alpha + Y\,dX) = 0} \quad \textbf{(I.8)}$$

The quantity $\int (\mathrm{P\,d\alpha + Y\,dX})$ is therefore an exact differential. According to Euler's reciprocity relation, this leads to:

Hence, X and Y can be selected with some degree of flexibility, provided they satisfy the aforementioned condition; in such instances, the enclosed area within the diagram will remain proportional to the work [13].

I.7.1.The Emagram 761

The Emagram is a specialized thermodynamic diagram characterized by its construction using an oblique coordinate system set at a 45° (x,y) Within this representation, the relationship between the oblique is(X,Y) coordinates and the conventional rectangular coordinates established through specific geometric transformations.

$$Y = \frac{y}{\sqrt{2}} \qquad \text{(I.9)}$$

$$X = x + \frac{y}{\sqrt{2}} = x + Y$$

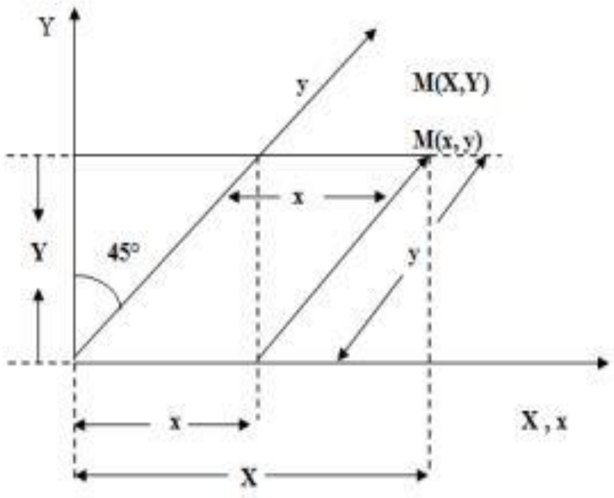

Figure (I.6): Emagram in rectangular coordinate [13].

- Horizontal Coordinate Analysis X:

The horizontal position on the Emagram is primarily determined by temperature. When T_0 is designated as the reference temperature at the origin, the horizontal component x can be expressed as:

$$T = T_0 + x \quad \Rightarrow \quad x = \alpha \times (T - T_0) \qquad \text{(I.10)}$$

T : temperature, **T_0:** reference temperature, **$t = T - T_0$** : temperature deviation

α : scaling constant

Consequently, the overall rectangular horizontal coordinate X integrates both the temperature and the vertical displacement, yielding:

$$X = x + Y = \alpha \times t + Y \qquad \text{(I.11)}$$

- Vertical Coordinate Analysis Y:

The vertical coordinate Y exhibits a proportional relationship with the logarithm of pressure, structured as follows:

$$\mathbf{Y = b \times \log_{10} \frac{p}{p_0}} \qquad \text{(I.12)}$$

To align with the fundamental atmospheric property where pressure decreases with increasing altitude, the Y-axis is oriented to indicate decreasing pressure upwards. Standard reference values are typically established with P_0 at 1000 hPa and P at 100 hPa.

- Scale Determination:

The scaling factors, denoted as 'a' and 'b', are assigned specific numerical values to ensure the practical utility of the diagram. The horizontal scale, 'a', is set at 4 mm. The vertical scale, 'b', is defined as the physical distance in millimeters that separates the 1000 hPa level from the 100 hPa level. For this particular model, 'b' is empirically determined to be 350 mm. Given that the logarithmic ratio between these two specified pressure levels is the vertical distance Y effectively corresponds to the scaling factor 'b', thereby establishing the fundamental dimensions of the Emagram [13].

$$\boldsymbol{log_{10}\frac{p}{p_0} = log_{10}\frac{1000}{100} = log_{10}10 = 1}$$

We obtain the following scales:

Along the Y-axis:

Thus: $\boldsymbol{Y(mm) = 350.log_{10}\left(\frac{1000}{P}\right) = 350(3 - log_{10}(P))}$

$$\mathbf{Y(mm) = 1050 - 350log_{10}(P)} \qquad \textbf{(I.13)}$$

Along the X-axis:

$$\mathbf{X\,(mm) = 4\,t + Y} \qquad \textbf{(I.14)}$$

Where: $t = T - T_0$ represents the temperature deviation.

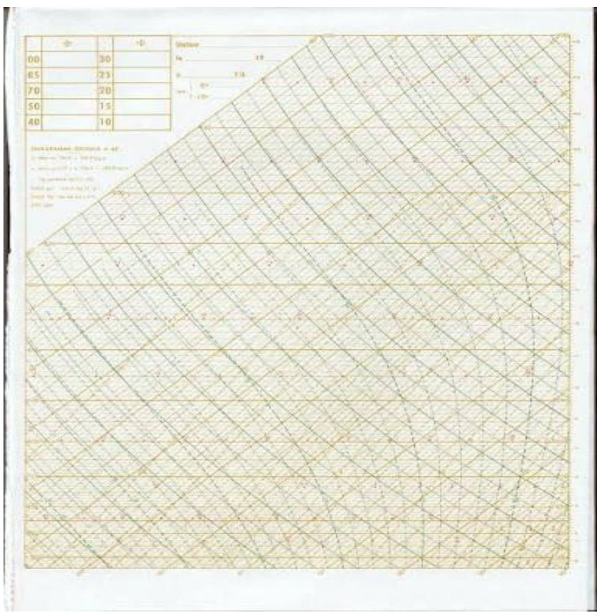

Figure (I.7): Emagram761 [14].

I.7.1.1.Orientation of Fundamental lines

The Emagram 761 delineates several fundamental isolines, each representing distinct thermodynamic variables:

- **Isobars (hPa):** These are presented as continuous horizontal lines, typically in a bistre (yellowish-brown) hue. Pressure values exhibit a logarithmic decrease towards the upper portion of the diagram, indicating that higher pressure levels correspond to lower altitudes.

- **Isotherms (°C):** Depicted as continuous bistre lines, these are oriented at a 45° inclination and are indexed along the horizontal axis (abscissa).

- **Dry Adiabats:** These curves illustrate the adiabatic transformations of dry air parcels, serving as lines of constant potential temperature. They appear as continuous green oblique curves. Their negative slope signifies the cooling that accompanies an air parcel's ascent to lower pressure levels, which is a consequence of adiabatic expansion. Progression from left to right along these curves indicates an increase in potential temperature.

- **Saturated Adiabats:** Also referred to as "pseudo-adiabats," these curves represent transformations occurring under saturated adiabatic conditions. Should an air parcel attain and sustain saturation, its thermodynamic state on the Emagram will follow one of these specific curves. Each pseudo-adiabat is indexed by the temperature it exhibits at its intersection with the 1000 hPa isobar. This specific value defines the wet-bulb potential pseudo-adiabatic temperature, which is commonly denoted as $\theta'w$.

- **Saturation Mixing Ratio Lines:** These lines indicate a constant saturation mixing ratio (rw). Each curve is labeled with its corresponding rw value, expressed in grams of water vapor per gram of dry air (g/g) [15].

I.7.2.The SkewT /log p

Atmospheric stability plays a fundamental role in the development of clouds, precipitation, and severe weather phenomena such as thunderstorms and tornadoes. To evaluate this stability, meteorologists rely on aerological soundings, which provide vertical profiles of temperature, humidity, and wind. Among the most widely used thermodynamic tools for this purpose is the Skew-T logP diagram (pseudo-adiabatic representation), which allows a detailed characterization of the vertical thermal structure of the atmosphere. An illustrative example of this diagram is shown in Figure I.8. Instability indices (CAPE, CIN, LI, K-index, etc.) are derived from it and provide a direct quantification of thunderstorm potential. Mastering this diagram is essential for anyone involved in meteorology, whether in operational forecasting, research, or aviation practice. The coordinate system is semi-logarithmic, where pressure (p) is plotted on a logarithmic vertical axis, while temperature (T) is represented on the horizontal axis. The term “Skew-T” refers to the intentional tilting of isotherms, which are drawn as oblique lines to improve the readability and analysis of atmospheric profiles [13].

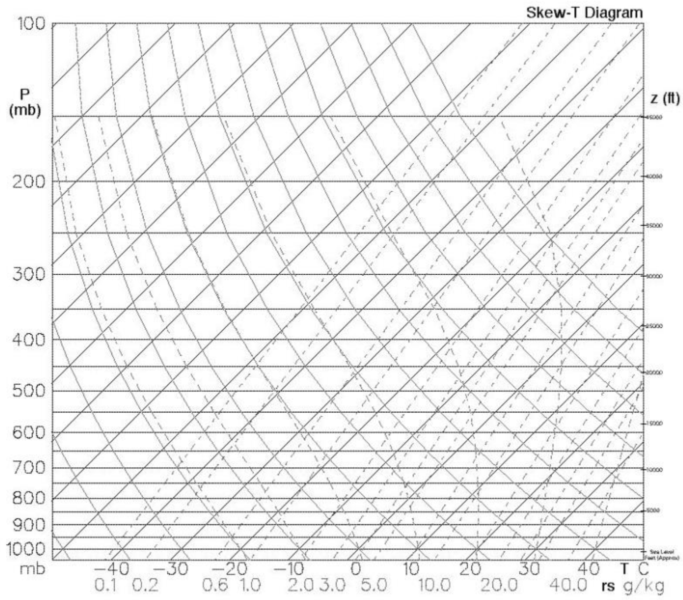

Figure (I.8): Skew-T diagram [14].

I.7.2.1.Orientation of the fundamental lines

The Skew-T diagram features a distinct arrangement of isolines crucial for evaluating atmospheric stability and related processes. These include:

- Isobars (hPa): which appear as horizontal blue lines indexed along the ordinate, reflecting the logarithmic decrease of pressure with altitude—that is, higher pressure values are situated at lower elevations.

- Isotherms (°C): shown as oblique blue lines indexed along the abscissa, contribute to the diagram's unique "skewed" configuration, enhancing the differentiation of various thermal profiles.

- Dry Adiabats: are represented by oblique green curves, illustrating the adiabatic transformations of dry air parcels and signifying lines of constant potential temperature θ. The slope of these curves indicates the cooling effect observed during the adiabatic expansion of an ascending air parcel. Potential temperature values increase as one moves horizontally from left to right across the diagram.

- Saturated Adiabats: also known as pseudo-adiabatic curves, are depicted as oblique blue curves. When an air parcel achieves and sustains saturation for instance, during ascent its state no longer adheres to a dry adiabat. Instead, its evolution follows a line of constant wet-bulb potential pseudo-adiabatic temperature, denoted as θ′w.

- Saturation Mixing Ratio Lines: are shown as purple curves. The mixing ratio (r), which quantifies the mass of water vapor relative to a unit mass of dry air, is determined by Dalton's Law of partial pressures: Where p represents the total atmospheric pressure, and e is the partial pressure of water vapor. Given that r is typically considerably less than 1, it is commonly expressed in grams of water vapor per kilogram of dry air (g/kg). On these thermodynamic diagrams, these particular lines denote the saturation mixing ratio, which corresponds to the maximum mass of water vapor that can exist at a specific temperature and pressure p [7].

I.8. Difference between the Skew-T logP) diagram and the Emagram 761

Both the Skew-T logP) diagram and the Emagram 761 are fundamental tools in meteorological analysis. While the Skew-T diagram finds primary application in Anglophone nations, particularly within the United States, the Emagram 761, originating from France, is predominantly employed in Francophone areas. Fundamentally, these graphical representations are distinct manifestations of a common thermodynamic diagrammatic framework, often referred to as an emagram [14] [16].

Key distinctions between these two widely used diagrams are noteworthy. Both share a design principle involving oblique coordinates set at a 45° angle, a feature intended to optimize graphical clarity and mitigate spatial constraints inherent in standard representations. However, their vertical axis definitions diverge significantly:

The Skew-T diagram utilizes the natural logarithm of pressure (logP), whereas the Emagram 761 employs the decimal logarithm of a pressure ratio, specifically $\log_{10}(P/P_0)$.

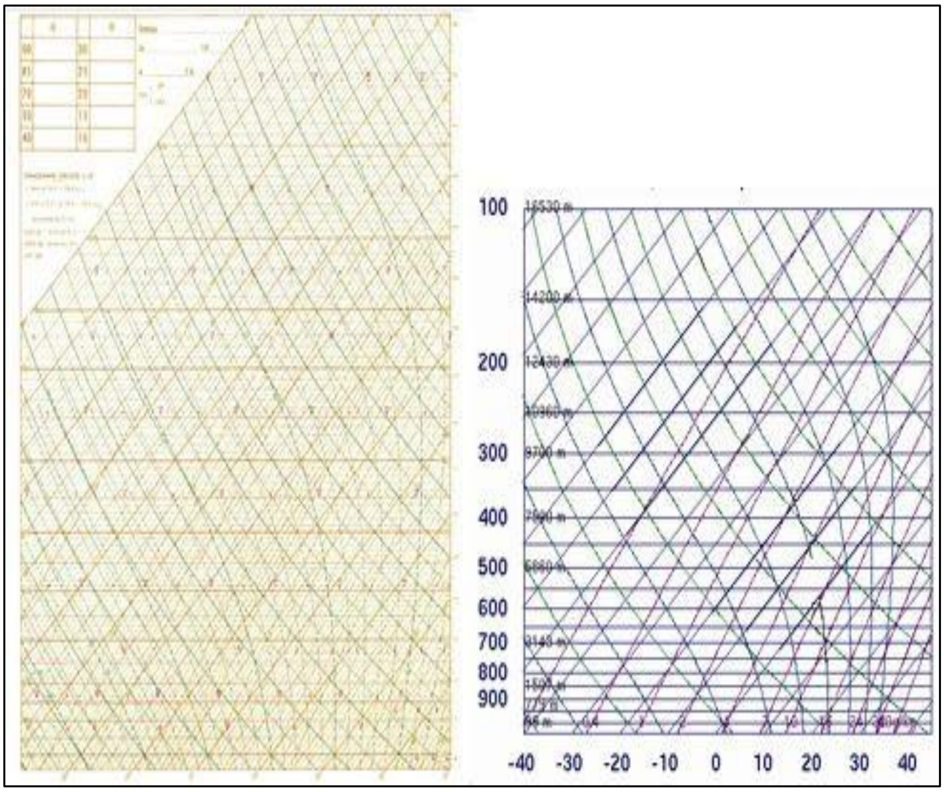

Figure (I.9): Emagram (left) and Skew-T logP diagram (right), showing the different graphical constructions used to represent atmospheric thermodynamic profiles [14].

I.9. Conclusion

This chapter has introduced the fundamental concepts of atmospheric stability, highlighting the physical and thermodynamic principles that govern vertical air motion. Key parameters such as temperature, pressure, and humidity, along with processes such as adiabatic transformations, play a central role in determining whether the atmosphere is stable, unstable, or conditionally unstable. Thermodynamic diagrams, including the Skew-T and the emagram, have been presented as essential tools for analyzing atmospheric profiles and interpreting real observations. These foundations are crucial for understanding cloud formation, convection, and a wide range of weather phenomena that will be examined in the following chapters. Furthermore, radiosonding has been presented as a fundamental and widely used method for investigating atmospheric conditions, providing direct and detailed vertical profiles of the atmosphere. However, atmospheric analysis is not limited to this approach alone. It can also rely on complementary data sources, such as reanalysis datasets and surface observations. These additional methods will be introduced and applied in Chapter III.

CHAPTER II:

STABILITY INDICES OF THE ATMOSPHERE

II.1. Introduction

This chapter focuses on atmospheric stability indices, which are essential tools for assessing the potential for convection and severe weather. These indices combine thermodynamic variables such as temperature, humidity, and pressure to provide quantitative measures of atmospheric instability. By using data from vertical soundings and thermodynamic diagrams, stability indices help identify conditions favorable for cloud development, thunderstorms, and other atmospheric phenomena. Understanding these indices is crucial for both weather analysis and forecasting.

II.2. Stability and instability of an air particle in the atmosphere

II.2.1. Atmospheric stability

Atmospheric stability denotes a thermodynamic state within the vertical atmospheric column that constrains vertical air motion. This condition is delineated by the inherent tendency of an air parcel, upon vertical displacement, to become cooler and consequently denser than its ambient environment, thereby initiating a negative buoyancy force that subsequently returns the parcel to its original elevation. In arid environments, this phenomenon is frequently observed during nocturnal surface inversions [9].

II.2.2. Atmospheric Instability

Atmospheric instability denotes a condition wherein the thermal stratification of the air column actively promotes and intensifies vertical air parcel movement. This state typically arises when the environmental lapse rate is significantly steeper than the adiabatic lapse rate. Under such circumstances, a rising air parcel tends to remain warmer and less dense than its ambient environment. These conditions consequentially generate positive buoyancy, which constitutes a fundamental factor driving convective activity and the formation of dust storms within arid regions [9].

II.3.Shematic illustration of atmospheric stability and instability processes

II.3.1.Equilibrium case of unsaturated air

Consider a layer of unsaturated air maintained in hydrostatic equilibrium, delineated by two distinct pressure levels, P_A and P_B ($P_A > P_B$), which correspond to altitude levels Z_A and Z_B ($Z_B > Z_A$). The temperatures at the base and the summit of this layer are denoted as t_A and t_B, respectively, and the temperature gradient across the layer is depicted as a linear segment connecting A and B.

Now, imagine a particle positioned at the base of this layer. Initially, this particle shares the same temperature, pressure, and density as its immediate surroundings. Should this particle be adiabatically elevated from pressure level P_A to P_B, without achieving saturation, its thermodynamic state at the upper level will transition to point C, characterized by temperature t_C [13].

Let us define the following parameters:

$$\Gamma_{aP} = \frac{T_C - T_A}{Z_B - Z_A} \quad \textbf{(II.1)}$$

$\boldsymbol{\Gamma_{aP}}$: Represents the rate of temperature change of an air parcel moving adiabatically, No heat exchange with the environment ($\Gamma a_P \approx -9.8$ °C/km)

$$\Gamma_{aE} = \frac{T_B - T_A}{Z_B - Z_A} \quad \textbf{(II.2)}$$

$\boldsymbol{\Gamma_{aE}}$ **:** Represents the actual temperature gradient of the atmosphere

Under these conditions, one of the subsequent equilibrium states may manifest [13].

Case 1: Stable Equilibrium (Figure II.1)

If $t_C < t_B$, it implies that $\theta_A < \theta_B$, and consequently, $\Gamma_{aP} > \Gamma_{aE}$. In this scenario, the environmental temperature profile exhibits a gentler slope compared to the dry adiabatic lapse rate, and the state curve is oriented to the right of the dry adiabat originating from A.

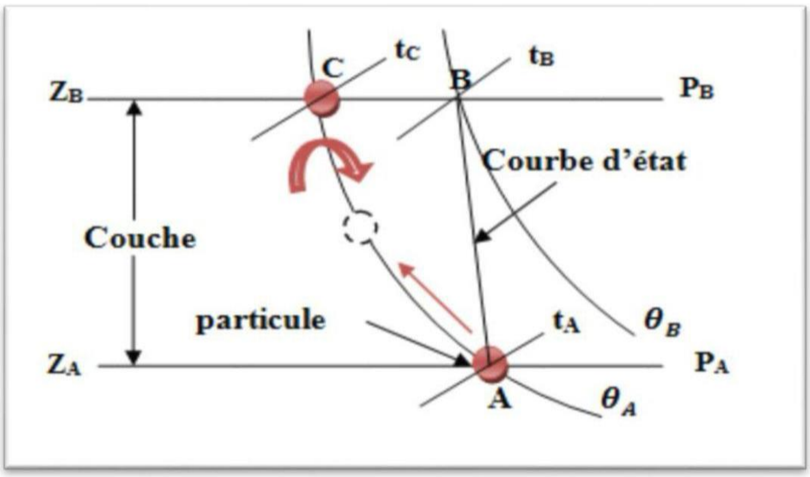

Figure (II.1): Stable Equilibrium [13].

Upon reaching pressure level P_B, the particle possesses a temperature lower than that of the surrounding air, leading to a correspondingly higher density. This density difference induces a tendency for the particle to revert to its initial position, thereby signifying a state of stable equilibrium [13].

Case 2: Unstable equilibrium (Figure II.2)

Should the condition $t_C > t_B$ hold, implying that $\theta_A > \theta_B$ and $\Gamma_{aP} < \Gamma_{aE}$ the environmental temperature profile is observed to be steeper than the dry adiabatic lapse rate. Consequently, the state curve is positioned to the right of the dry adiabat originating from A.

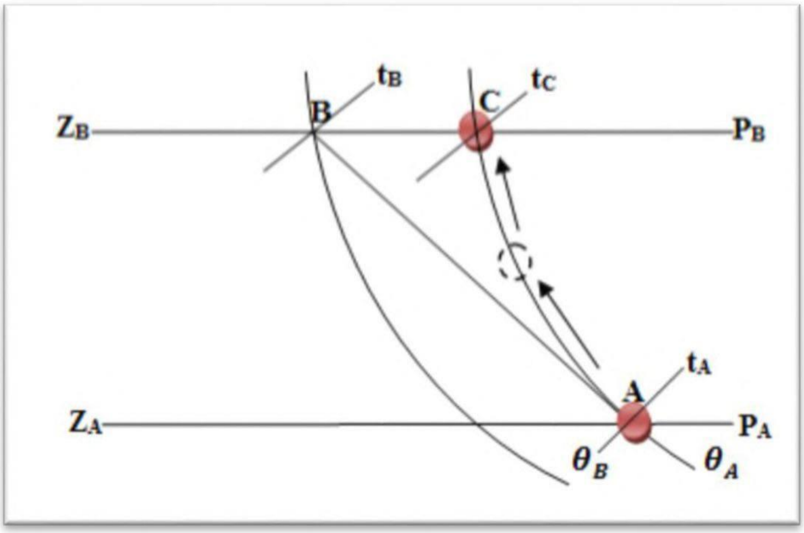

Figure (II.2): Unstable equilibrium [13].

When the particle ascends to the pressure level P_B, its temperature surpasses that of the surrounding air, resulting in a reduced density. This density differential subsequently promotes continued ascent, which is indicative of an unstable equilibrium [13].

Case 3: Neutral equilibrium (Figure II.3)

Neutral equilibrium is observed when $t_C = t_B$, a condition that necessitates $\theta_A = \theta_B$ and $\Gamma_{aP} = \Gamma_{aE}$ In this state, regardless of a particle's vertical displacement whether through forced ascent or descent within the interval between P_A and P_B, its temperature at the new altitude will consistently match that of the ambient air. This thermal congruence, in turn, ensures an equivalent density. Consequently, the particle exhibits no inherent tendency to ascend further or to revert to its original position; such an equilibrium is thus characterized as neutral or indifferent .This condition may manifest as a result of the admixture of distinct air masses or the mechanical homogenization of an air mass, often induced by turbulent or windy conditions. The particle attains thermal equilibrium with its ambient environment via heat exchange mechanisms; consequently, the vertical displacement process in these scenarios is fundamentally non-adiabatic [13].

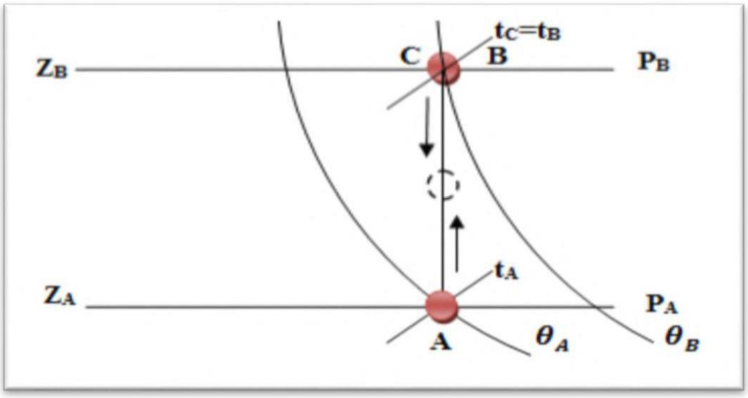

Figure (II.3): Neutral equilibrium [13].

II.3.2.Equilibrium cases of saturated air

It is sufficient, in the previous case, to replace the adiabatic potential temperatures θ with the pseudo-adiabatic (wet-bulb) potential temperatures θ', and the dry adiabatic lapse rates Γa with the saturated adiabatic lapse rates Γs.

This leads to the following cases [13]:

Case 1: Stable equilibrium (Figure II.4)

If $t_C < t_B$, , then $\theta'_{WA} < \theta'_{WB}$ and $\Gamma_{sP} > \Gamma_{sE}$ in this case, the equilibrium is stable.

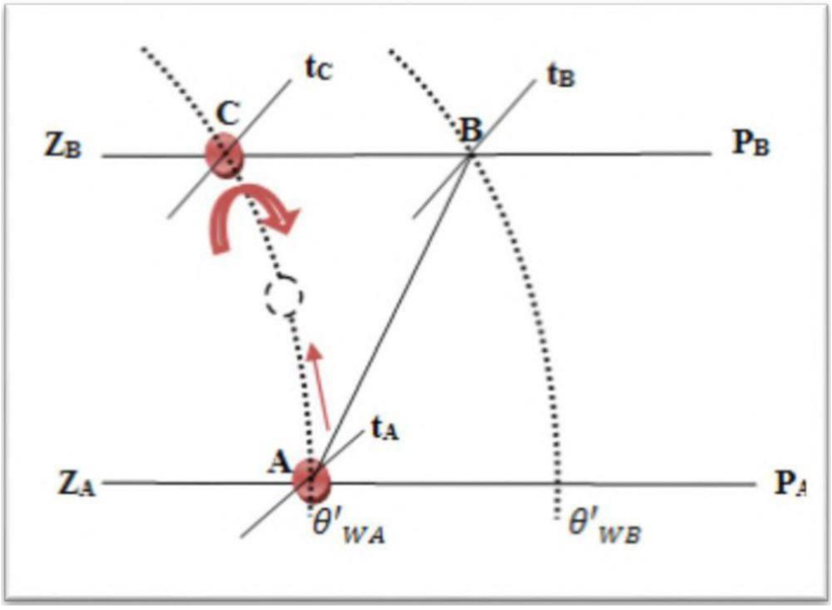

Figure (II.4): Stable equilibrium [13].

Case 2: Unstable equilibrium (Figure II.5)

If $t_C > t_B$, , then $\theta'_{WA} > \theta'_{WB}$ and $\Gamma_{sP} < \Gamma_{sE}$ in this case, the equilibrium is unstable.

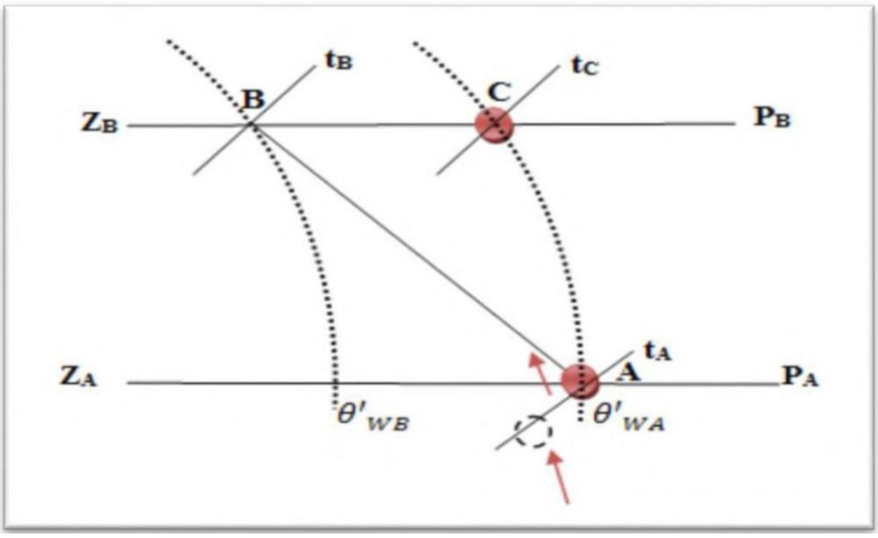

Figure (II.5): Unstable equilibrium [13].

Case 3: Neutral equilibrium (Figure II.6)

If $t_C = t_B$, , then $\theta'_{WA} = \theta'_{WB}$ and $\Gamma_{sP} = \Gamma_{sE}$,in this case, the equilibrium is neutral or indifferent.

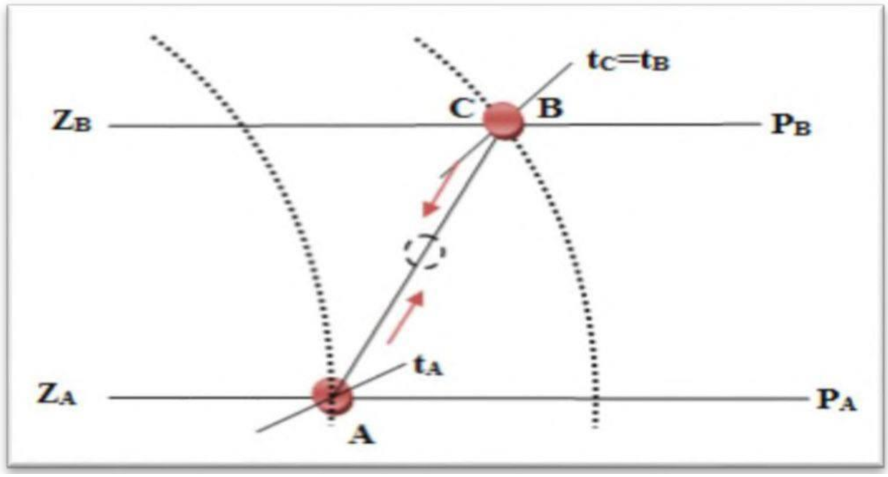

Figure (II.6): Neutral equilibrium [13].

II.3.3. Conditional (or latent) instability of an air parcel

Conditional instability refers to a atmospheric state where unsaturated air parcels maintain stability, though this condition transitions to instability once saturation is achieved. This particular state is recognized as a prerequisite for the formation of convective storms, provided sufficient moisture is available [2].

II.4. Main levels that can be reached by an adiabatically lifted air parcel

As is well known, most atmospheric indices relevant to stability analysis can be derived from the present case using the SkewT–logP diagram. This thermodynamic tool allows tracking the behavior of an air parcel as it is lifted adiabatically through the atmospheric column.

II.4.1. Lifting Condensation Level (LCL)

The Lifting Condensation Level represents the altitude where a parcel of air achieves saturation when subjected to mechanical or orographic lifting from the surface. During this ascent, the air parcel cools at the dry adiabatic lapse rate until its temperature equates with its dew point. meteorologically, the LCL functions as a reliable predictor for the base height of cumuliform clouds, typically arising from dynamic forcing mechanisms, including frontal boundaries or topographic uplift [17].

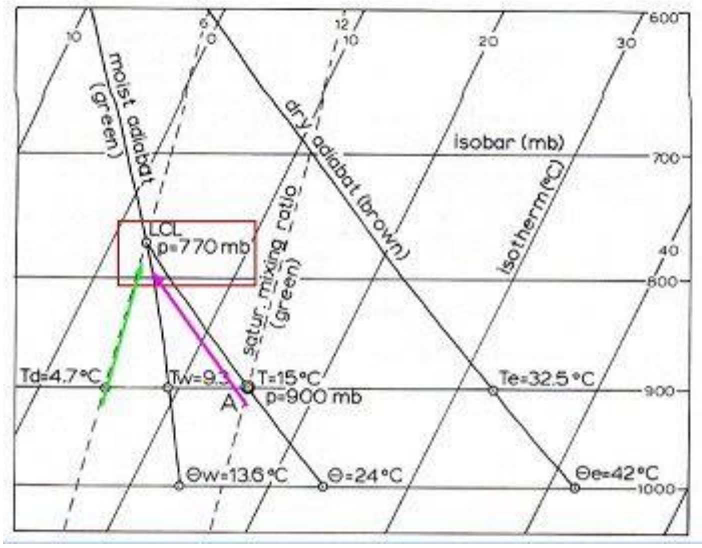

Figure (II.7): Illustration of the Lifted Condensation Level (LCL) on a Skew-T Diagram [18].

II.4.2. Convective Condensation Level (CCL)

The Convective Condensation Level denotes the altitude where condensation initiates, primarily driven by diurnal solar insolation warming the Earth's surface. In contrast to the LCL, the CCL is attained when surface temperatures ascend to a specific critical Convective Temperature (Tc), thereby enabling the air parcel to rise buoyantly without requiring exogenous mechanical support. This particular level is principally employed to ascertain the base of convective clouds, such as thermals, that develop within unstable, thermally-driven air masses [17].

II.4.3. Level of Free Convection (LFC)

The Level of Free Convection identifies the atmospheric altitude above which a saturated air parcel exhibits a temperature higher than, and consequently a density lower than, its ambient surroundings. Once this threshold is surpassed, the air parcel acquires positive buoyancy, facilitating a self-sustaining vertical ascent unassisted by additional external forcing mechanisms. Consequently, the LFC signifies the transition from an externally forced upward motion to a regime of free convection, serving as a pivotal determinant for the initiation and progression of deep convective systems and thunderstorms [17].

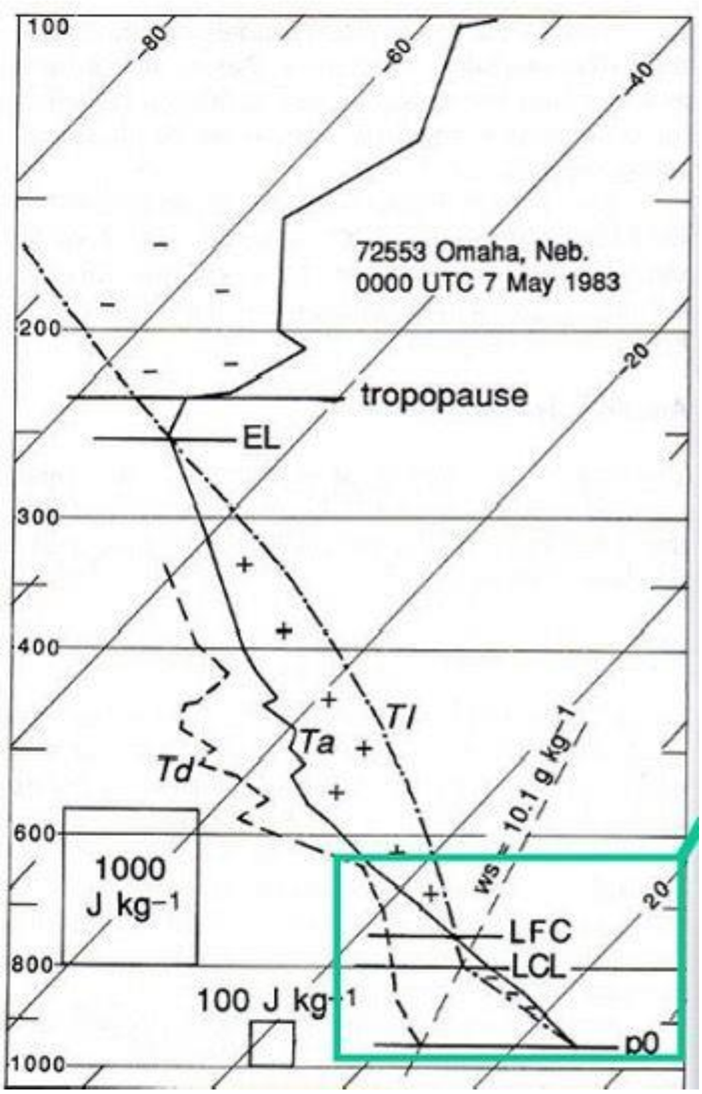

Figure (II.8): Determination of the Level of Free Convection (LFC) on a Skew-T Diagram [18].

II.4.4. Equilibrium Level (EL)

The Equilibrium Level denotes the altitude at which a buoyantly rising air parcel, during its free convective ascent, attains thermal equilibrium with the surrounding environment. Subsequently, at this elevation, the parcel ceases its upward buoyancy and becomes thermally stable with respect to its immediate surroundings. In meteorological contexts, the EL is employed to estimate the maximal vertical development of clouds, thereby effectively defining an upper limit for thunderstorm tops and influencing the characteristic formation of anvil structures [17].

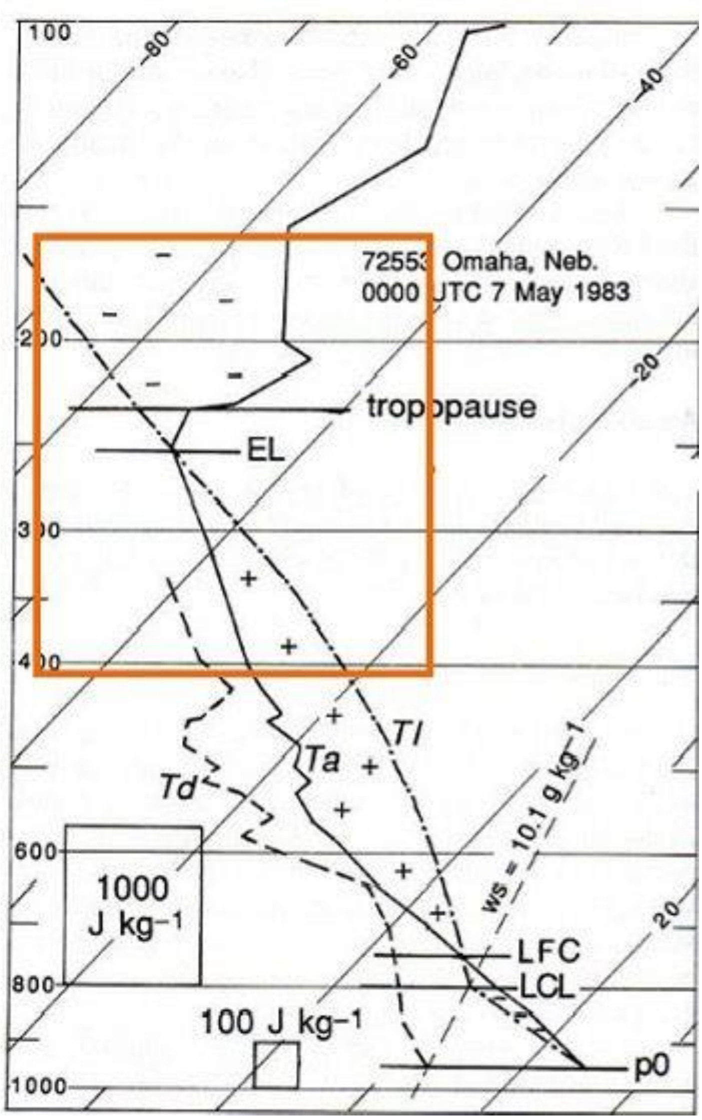

Figure (II.9): Determination of the Equilibrium Level (EL) on a Skew-T Diagram [18].

II.5. Stability indices

Atmospheric stability indices are diagnostic tools designed to quantify the convective potential of an air mass. By utilizing data from radiosonde soundings or numerical weather prediction (NWP) models, these indices evaluate temperature, humidity, and vertical lapse rates to provide a numerical representation of instability [19].

II.5.1. Showalter Index (SI)

The Showalter Index is a localized measure of buoyancy that evaluates the potential for elevated convection. It is calculated by lifting a theoretical air parcel dry-adiabatically from the 850 hPa level to its Lifted Condensation Level (LCL), and subsequently following the saturated adiabat to the 500 hPa level [19].

$$SI = t - t' \text{ (en °C)} \qquad \textbf{(II.3)}$$

Where:

t = ambient air temperature, read from the environmental sounding curve at the 500 hPa level

t′ = temperature reached at 500 hPa by an air parcel initially at 850 hPa, after ascending adiabatically: first following the dry adiabat up to the lifting condensation level (LCL), then the saturated pseudo-adiabat up to 500 hPa

- **Interpretation**: A more negative value indicates higher instability generally , values below **+3** suggest convective potential, while values below **-3** are indicative of severe thunderstorm environments [19].

II.5.2.K-Index (KI)

George's K-Index is a comprehensive stability metric that accounts for three critical factors: the vertical lapse rate, lower-tropospheric moisture content, and the vertical extent of the humid layer [19].

$$\boldsymbol{KI = (T_{850} - T_{500}) + Td850 - (T_{700} - T_{d700})} \qquad \textbf{(II.4)}$$

Where:

$\mathbf{T_{850}}$, $\mathbf{T_{700}}$, $\mathbf{T_{500}}$, $\mathbf{T_{d700}}$ = ambient air temperature at 850, 700, and 500 hPa, respectively.

$\mathbf{T_{d850}}$, $\mathbf{T_{d700}}$ = deux point temperature at 850 and 700 hPa, respectively.

- **Interpretation:** A value below 20 suggests a negligible probability of convection, whereas values exceeding 35 correlate with widespread thunderstorm activity. However, its effectiveness varies between air masses due to shifting lapse rate climatologies [19].

II.5.3. Lifted Index (LI)

The Lifted Index assesses buoyancy by comparing the temperature of a surface-based parcel lifted to 500 hPa with the ambient temperature at that level [19].

$$\boldsymbol{LI = T5 - TS \ (en°C)} \qquad \textbf{(II.5)}$$

Where:

$\mathbf{T_5}$= dry-bulb temperature (environmental air) at 500 hPa

T_S = temperature of a surface air parcel lifted adiabatically to the 500 hPa level.

- Interpretation: Negative values signify instability. Values lower than -6 suggest a high potential for severe convective development [19].

II.5.4. SWEAT Index

The SWEAT Index, or Severe Weather Threat Index, is calculated as follows [19]:

$$\boldsymbol{SWEAT = 12 * T_{d850} + 20 \cdot (TTI - 49) + 2 * f_{850} + f_{500} + 125 * [sin(dd_{500} - dd_{850}) + 0.2]} \quad \textbf{(II.6)}$$

Where:

T_{d850}: point temperature at 850 hPa in °C (if $T_{d850} < 0$, then $1 * T_{d850} = 0$)

TTI: Total Totals Index in °C (If TTI < 49, then $20 * (TTI - 49) = 0$)

If ($dd_{500} < dd_{850}$), then 125*[sin (dd500 − dd850) + 0.2] = 0 12*[sin ($dd_{500} - dd_{850}$) +0.2] =0

f_{850}: wind speed at 850 hPa, in knots

f_{500}: wind speed at 500 hPa, in knots

sin ($dd_{500} - dd_{850}$): sine of the difference between wind directions at 500 hPa and 850 hPa

- Interpretation: High SWEAT values indicate an increased likelihood of severe weather events, including intense thunderstorms, hail, and tornadoes. Conversely, low values generally indicate stable weather conditions, characterized by limited thermal activity. The integration of humidity, instability, and wind shear within this index makes it a valuable diagnostic tool for assessing the probability of severe thermal weather[19].

II.5.5. Total Totals Index (TTI)

The TTI is a combination of Vertical Totals (VT) and Cross Totals (CT), used to identify environments conducive to severe weather[19].

$$\boldsymbol{TTI = (T_{850} - T_{500}) + (T_{d850} - T_{500})\ en°C} \quad \textbf{(II.7)}$$

Where:

T_{850}: temperature at 850 hPa

T_{500} : temperature at 500 hPa

$T_{d\,850}$: point temperature at 850 hPa

- Interpretation: Values exceeding 50 are typically associated with severe convective storms [19].

II.5.6. Convective Available Potential Energy (CAPE)

Convective Available Potential Energy (CAPE) represents the integrated buoyant energy available to an air parcel as it ascends through the atmosphere. It is a key indicator of atmospheric instability and the potential intensity of convective updrafts.

$$CAPE = \int_{LFC}^{EL} g.\left(\frac{T_{parcel}-T_{env}}{T_{env}}\right)\mathrm{dz} \qquad (J\,.\,Kg^{-1}) \qquad \textbf{(II.8)}$$

Where:

T_{VP}: virtual temperature of the air parcel

T_{Ve}: virtual temperature of the environment

g : cceleration due to gravity

dz : infinitesimal vertical displacement

(LCL): Lifting Condensation Level

(EL): Equilibrium Level

- Interpretation: Higher CAPE values indicate greater atmospheric instability and stronger potential for convective development and severe thunderstorms. Low values correspond to stable atmospheric conditions with weak or suppressed convection [19].

II.5.7.Convective Inhibition (CIN)

Convective Inhibition (CIN) represents the amount of energy that prevents an air parcel from rising from the surface to the Level of Free Convection (LFC). It acts as a stabilizing layer that suppresses convective initiation[19].

$$CIN = \int_{Surface}^{LFC} g.\left(\frac{T_{parcel}-T_{env}}{T_{env}}\right) \qquad (J.Kg-1) \qquad \textbf{(II.9)}$$

where:

g : is the acceleration due to gravity,

T_{VP}: virtual temperature of the air parcel

T_{Ve}: virtual temperature of the environment

Z_0 is the starting level (usually near the surface),

Z_{LFC} is the Level of Free Convection

- Interpretation : Negative CIN values indicate strong atmospheric stability and suppression of convection, while weak or near-zero values suggest that only minimal external forcing is required to initiate convective development [19].

CHAPTER III:

ANALYSIS OF ATMOSPHERIC STABILITY INDICES

III.1. Introduction

To better understand and forecast meteorological phenomena, the atmosphere is continuously monitored using dense surface observation networks. However, due to the strong spatial variability of atmospheric processes, surface measurements alone are not sufficient. In this context, although several observational methods such as radiosonde measurements, satellite observations, and ground-based data are commonly used for atmospheric analysis, the limited availability of in-situ observations led to the use of ERA5 reanalysis data in this study. This chapter focuses on the analysis of a pluvio-orageous event over the regions of Laghouat and Ouargla during the period from 12 to 15 April 2024, using upper-air data to investigate the atmospheric conditions associated with this event.

III.2. Geographical and climatological characteristics of the Laghouat and Ouargla regions

III.2.1.The region of Laghouat

The wilaya of Laghouat is situated in the central-northern part of the Algerian Sahara, serving as a transition zone between the northern steppe and the southern desert regions. It is characterized by an arid to semi-arid climate, with hot summers (often above 40°C) and cold winters where temperatures may drop close to 0°C. Occasional dust and sand storms are also observed. It is limited by (see Figure III.1)

To the North, the wilaya of Djelfa

To the East, the wilayas of Biskra and Ouargla

To the West, the wilaya of El Bayadh

To the South, the wilayas of Ghardaïa and Ouargla.

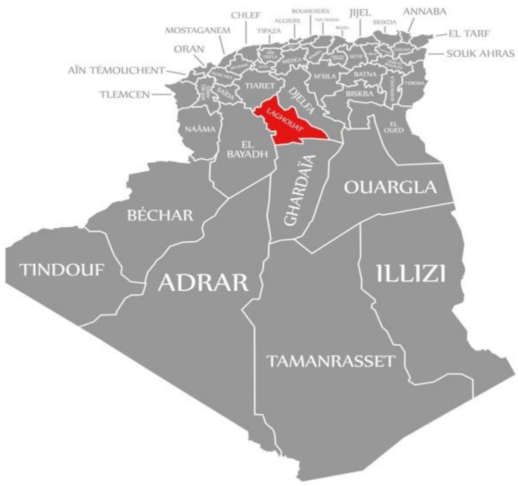

Figure(III.1):Geographical location of the Laghouat region in Algeria

III.2.2. The region of Ouargla

The region of Ouargla is located in the southeast of Algeria, deep within the Saharan desert. It covers a vast area characterized by arid environmental conditions. The region is known for its desert climate, with extremely hot summers often exceeding 45°C and mild to cool winters. Sandstorms are frequent and can be strong and persistent. It is bordered by (see Figure III.2)

To the North, the wilayas of El Oued and Djelfa

To the East, the wilaya of Illizi

To the West, the wilayas of Ghardaïa and Laghouat

To the South, the borders of Tunisia and Libya

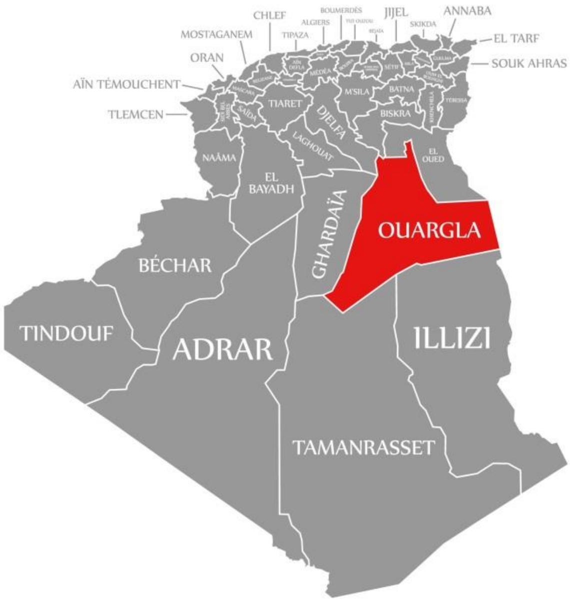

Figure (III.2): Geographical location of the Ouargla region in Algeria

III.3. Data Sources and Methodology

To ensure a comprehensive assessment of atmospheric stability over the regions of Laghouat and Ouargla, this study relies exclusively on ERA5 reanalysis data provided by the European Centre for Medium-Range Weather Forecasts (ECMWF). This dataset offers consistent and high-resolution atmospheric variables on multiple pressure levels, allowing a detailed characterization of the vertical thermodynamic structure during the studied convective event. Therefore, ERA5 provides all the necessary information to compute and analyze atmospheric stability indices such as CAPE, CIN, and LI and others.

These measurements are fundamental for constructing thermodynamic diagrams, particularly the Skew-T log-P diagram, which enables an in-depth analysis of the vertical thermal and moisture stratification, as well as atmospheric stability conditions on the day of the event.The methodological approach begins with plotting the vertical profiles of air temperature (T) and dew point temperature (Td) on the thermodynamic diagram.

Based on these profiles, several key atmospheric stability indices are computed, including Convective Available Potential Energy (CAPE), Convective Inhibition (CIN), Lifted Index (LI), K Index (KI), and Total Totals Index (TTI). These indices are subsequently analyzed and compared in order to evaluate their effectiveness in diagnosing atmospheric instability and forecasting convective activity associated with the studied episode.ERA5 reanalysis data, generated through the assimilation of a wide range of observations into numerical weather prediction models, provide a consistent and spatially continuous reconstruction of the atmospheric state on a global grid over extended time periods. This makes them particularly valuable for synoptic-scale analysis and for ensuring temporal and spatial coherence when comparing atmospheric conditions across different events.

III.4. Presentation of ERA5 reanalysis data from the ECMWF

III.4.1. ERA5 reanalysis data of Laghouat region

The ERA5 reanalysis data from the ECMWF (European Centre for Medium-Range Weather Forecasts) for the days 12, 13, and 14 of 2024, at 00:00 and 12:00 UTC for each day (corresponding to the beginning of the day and late morning), in Laghouat region are presented using the climatological Skew-T log-P diagram (see Figures III.3 a,b,c,d,e and f. below).

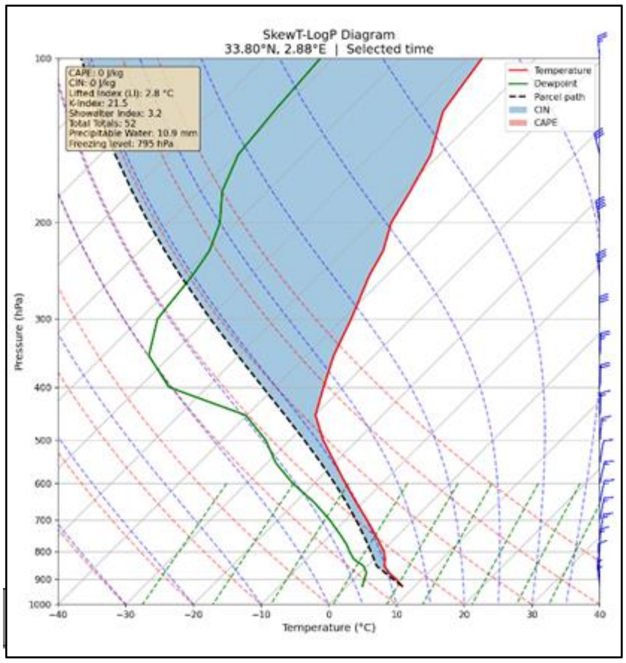
SkewT-LogP Diagram
33.80°N, 2.88°E | Selected time
CAPE: 0 J/kg
CIN: 0 J/kg
Lifted Index (LI): 2.8 °C
K-Index: 21.5
Showalter Index: 3.2
Total Totals: 52
Precipitable Water: 10.9 mm
Freezing level: 795 hPa
Temperature
Dewpoint
Parcel path
CIN
CAPE
Pressure (hPa)
Temperature (°C)

a

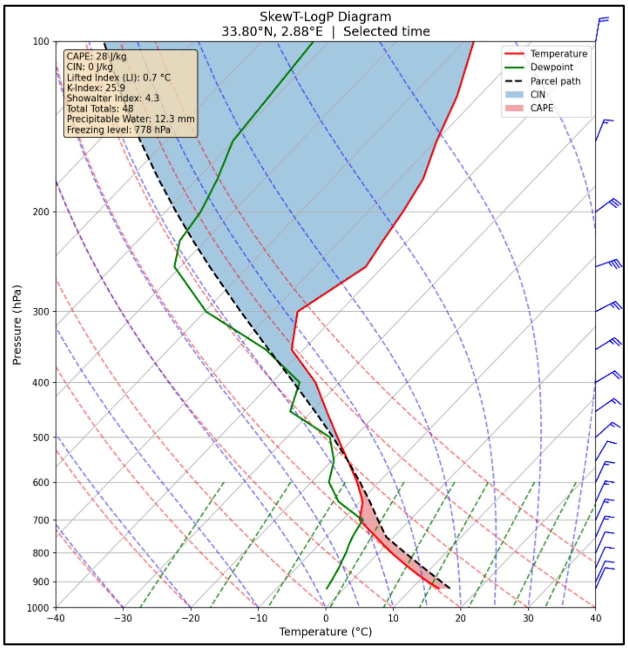
SkewT-LogP Diagram
33.80°N, 2.88°E | Selected time
CAPE: 28 J/kg
CIN: 0 J/kg
Lifted Index (LI): 0.7 °C
K-Index: 25.9
Showalter Index: 4.3
Total Totals: 48
Precipitable Water: 12.3 mm
Freezing level: 778 hPa
Temperature
Dewpoint
Parcel path
CIN
CAPE
Pressure (hPa)
Temperature (°C)

b

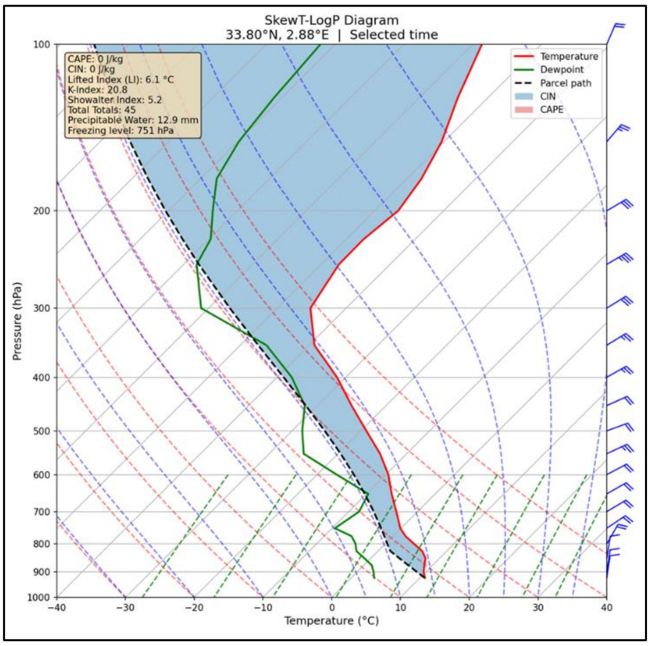
SkewT-LogP Diagram
33.80°N, 2.88°E | Selected time
CAPE: 0 J/kg
CIN: 0 J/kg
Lifted Index (LI): 6.1 °C
K-Index: 20.8
Showalter Index: 5.2
Total Totals: 45
Precipitable Water: 12.9 mm
Freezing level: 751 hPa
Temperature
Dewpoint
Parcel path
CIN
CAPE
Pressure (hPa)
Temperature (°C)

c

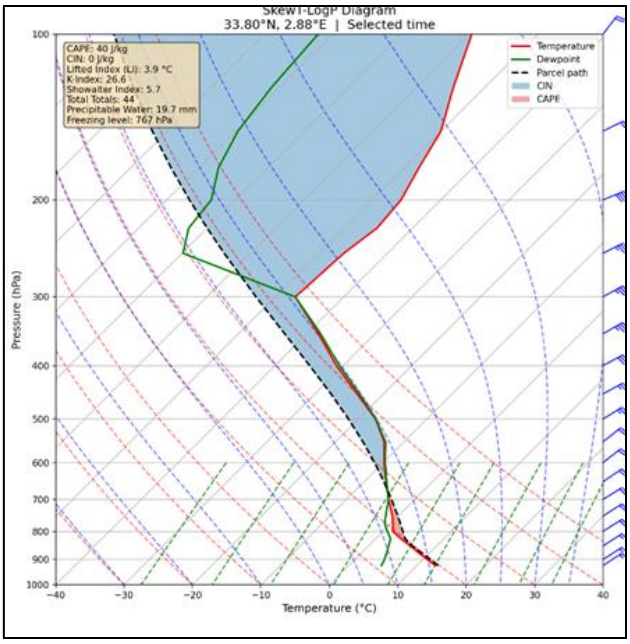
SkewT-LogP Diagram
33.80°N, 2.88°E | Selected time
CAPE: 40 J/kg
CIN: 0 J/kg
Lifted Index (LI): 3.9 °C
K-Index: 26.6
Showalter Index: 5.7
Total Totals: 44
Precipitable Water: 19.7 mm
Freezing level: 767 hPa
Temperature
Dewpoint
Parcel path
CIN
CAPE
Pressure (hPa)
Temperature (°C)

d

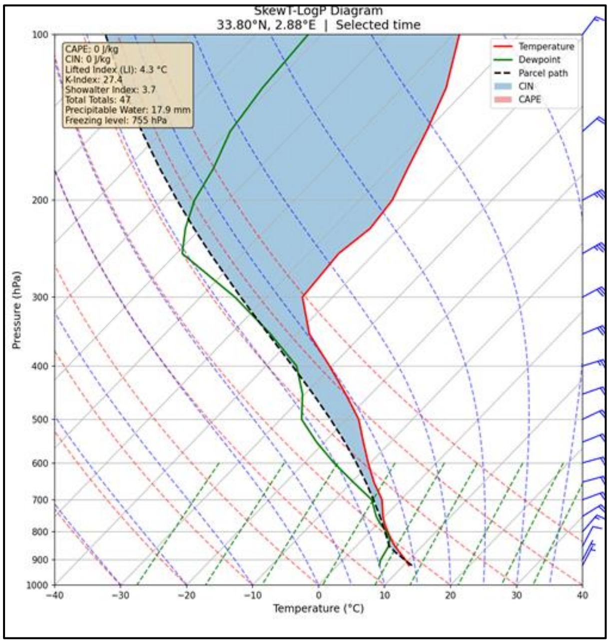

e

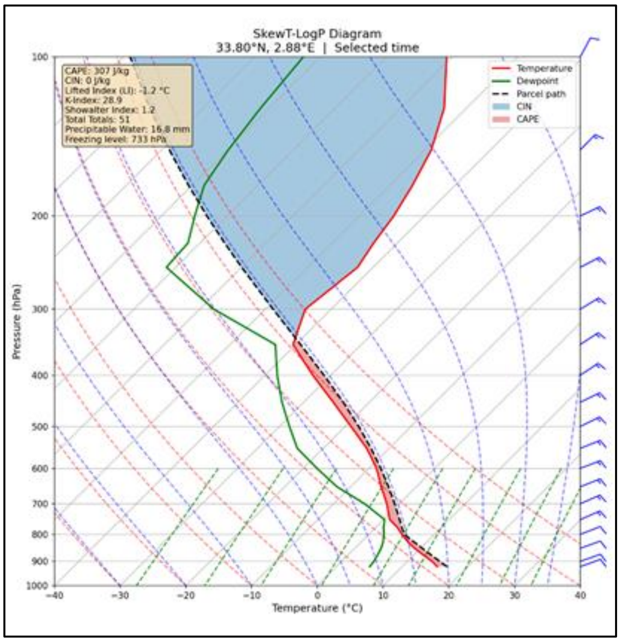

f

Figures (III.3): (a,b),(c,d),(e, f) Days of 12,13,14 /April 2024 for 00h and 12h UT respectively

III.4.1.1. Stability indices of the Laghouat region

Based on European Centre for Medium-Range Weather Forecasts ERA5 reanalysis data, the atmospheric indices are computed as follows:

TABLE (III.1): Stability Indices for 12 April 2024

Hour	CAPE (J/Kg)	CIN (J/Kg)	LI (°C)	KI	SI	TTI	Pre. wat.(mm)	F. le(hPa)
00h	0	0	2.8	21.5	3.2	52	10.9	795
12h	28	0	0.7	25.9	4.3	48	12.3	778

TABLE (III.2): Stability Indices for 13 April 2024

Hour	CAPE (J/Kg)	CIN (J/Kg)	LI (°C)	KI	SI	TTI	Pre. wat.(mm)	F. le(hPa)
00h	0	0	6,1	20,8	5,2	45	12,9	751
12h	40	0	3,9	26,6	5,7	44	19,7	767

TABLE (III.3): Instability Indices for 14 April 2024

Hour	CAPE (J/Kg)	CIN (J/Kg)	LI (°C)	KI	SI	TTI	Pre. wat.(mm)	F. le(hPa)
00h	0	0	4,3	27,4	3,7	47	17,9	755
12h	307	0	-1,2	28,9	1,2	51	16,9	733

Pre. wat.(mm) : Precipitable Water (mm)

F. le(hPa) : Freezing Level(hPa)

III.4.1.2. Interpretation of atmospheric stability of the Laghouat region

The day of April 12, 2024

- At 00:00 UTC, the atmosphere is stable, with CAPE = 0 J/kg, CIN = 0 J/kg, and a positive LI of 2.8°C, indicating a lack of convective potential. The K-index (21.5), SI (3.2), and TTI (52) also confirm stable conditions. The precipitable water (10.9 mm) is relatively low, supporting a dry atmospheric state.
- At 12:00 UTC, a slight decrease in stability is observed. The CAPE increases to 28 J/kg, while LI decreases to 0.7°C, indicating a transition toward near-neutral conditions. The K-index rises to 25.9 and precipitable water increases to 12.3 mm, suggesting a weak moistening and slight improvement in convective potential. However, the atmosphere remains generally stable with no significant convective risk.

The day of April 13, 2024

- At 00:00 UTC, the atmosphere is strongly stable, with CAPE = 0 J/kg, CIN = 0 J/kg, and a positive LI of 6.1°C, indicating a highly stable stratification and no convective potential. The K-index (20.8), SI (5.2), and TTI (45) further confirm unfavorable conditions for convection. The precipitable water (12.9 mm) remains low to moderate, consistent with a dry and stable atmospheric profile.
- At 12:00 UTC, a slight reduction in stability is observed. The CAPE increases to 40 J/kg, while LI decreases to 3.9°C, indicating a weak destabilization of the atmosphere. The K-index rises to 26.6 and precipitable water increases significantly to 19.7 mm, suggesting a moistening of the atmospheric column. However, despite this evolution, the atmosphere remains generally stable with only weak convective potential.

The day of April 14, 2024

➢ At 00:00 UTC, the atmosphere remains stable, with CAPE = 0 J/kg, CIN = 0 J/kg, and a positive LI of 4.3°C, indicating a strongly stable stratification. The K-index (27.4), SI (3.7), and TTI (47) are consistent with non-convective conditions. The precipitable water (17.9 mm) shows moderate moisture availability, but it is not sufficient to support convection.

➢ At 12:00 UTC, a marked destabilization occurs. The CAPE increases sharply to 307 J/kg, indicating the development of moderate convective potential, while the LI drops to -1.2°C, signaling an unstable atmosphere favorable for convection. The K-index (28.9) and TTI (51) also increase slightly, supporting this transition toward instability. The precipitable water (16.9 mm) remains sufficient to sustain moist processes, and the freezing level decreases to 733 hPa, consistent with enhanced vertical development potential. Overall, the atmosphere becomes significantly more favorable for convective activity at midday.

III.4.2.ERA5 reanalysis data of Ouargla region

The ERA5 reanalysis data from the ECMWF (European Centre for Medium-Range Weather Forecasts) for the days 12, 13, and 14 of 2024, at 00:00 and 12:00 UTC for each day (corresponding to the beginning of the day and late morning), in the Ouargla region are presented using the climatological Skew-T log-P diagram (see Figures III.4 g,h,I,j,k and l. below).

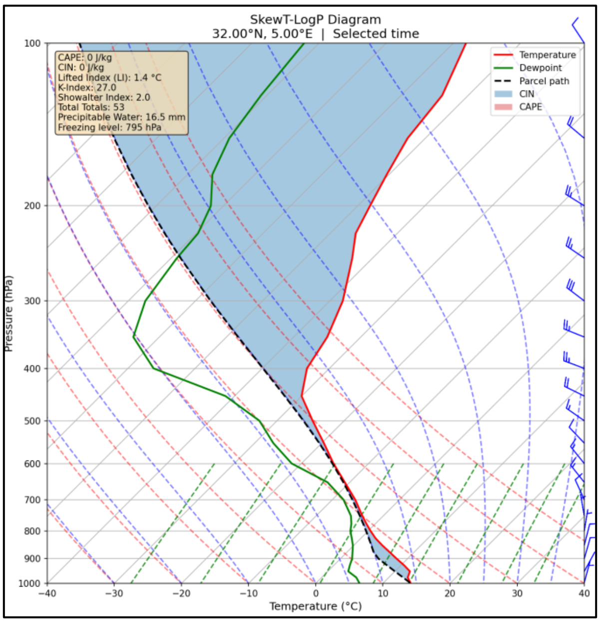

g

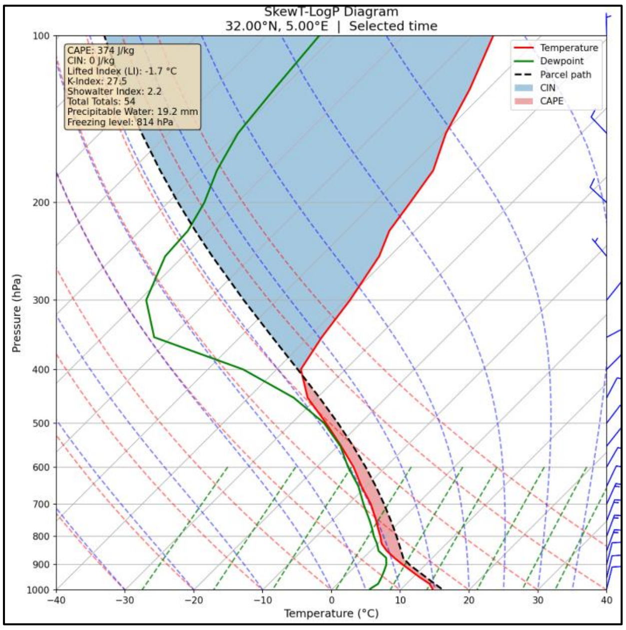

h

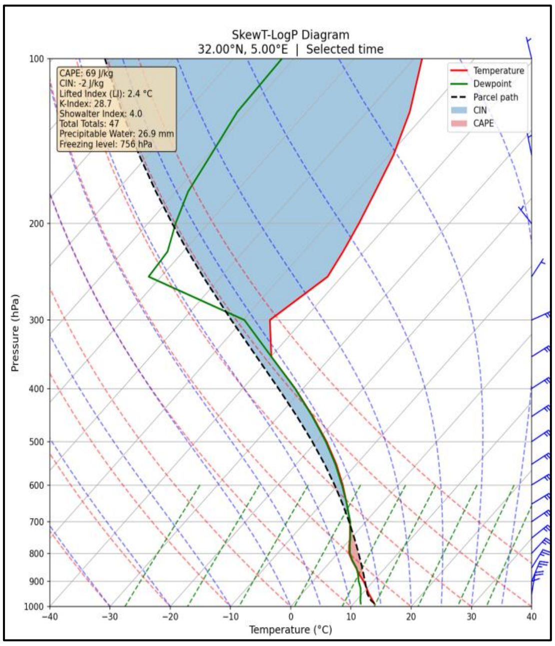

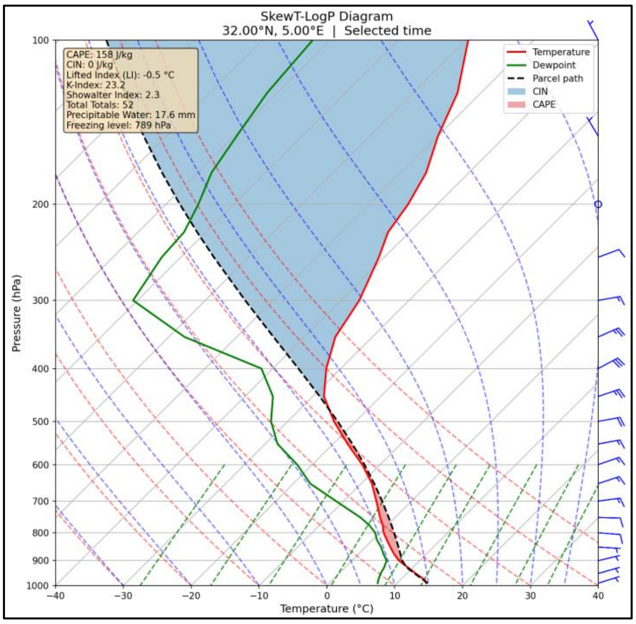

i **j**

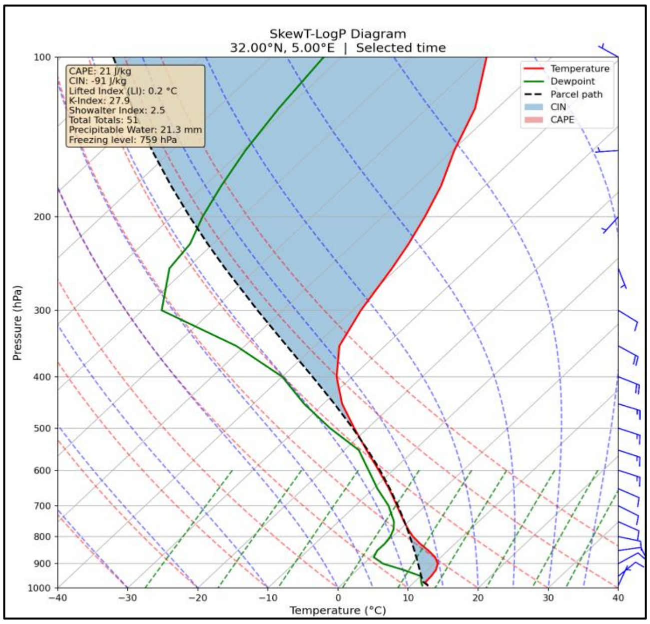

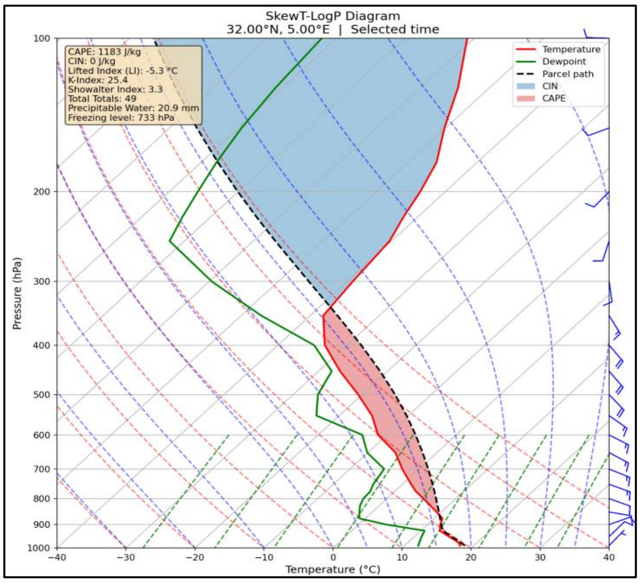

k **l**

Figures(III.4): (g,h),(i,j),(k, l) Days of 12,13,14 /April 2024 for 00h and 12h UTC respectively

III.4.2.1. Stability indices of the Ouargla region

TABLE (III.4):Stability Indices for 12 April 2024

Hour	CAPE (J/Kg)	CIN (J/Kg)	LI (°C)	KI	SI	TTI	Pre. wat.(mm)	F. le(hPa)
00h	0	0	1,4	27,0	2,0	53	16,5	795
12h	374	0	-1,7	27,5	2,2	54	19,2	814

TABLE (III.5): Stability Indices for 13 April 2024

Hour	CAPE (J/Kg)	CIN (J/Kg)	LI (°C)	KI	SI	TTI	Pre. wat.(mm)	F. le(hPa)
00h	69	-2	2,4	28,7	4,0	47	26,9	756
12h	158	0	-0,5	23,2	2,3	52	17,6	789

TABLE (III.6): Stability Indices for 14 April 2024

Hour	CAPE (J/Kg)	CIN (J/Kg)	LI (°C)	KI	SI	TTI	Pre. wat.(mm)	F. le(hPa)
00h	21	-91	0,2	27,9	2,5	51	21,3	759
12h	1183	0	-5,3	25,4	3,3	49	20,9	733

Pre. wat.(mm) : Precipitable Water (mm)

F. le(hPa) : Freezing Level(hPa)

III.4.2.2. Interpretation of atmospheric stability of the Ouargla region

The day of April 12, 2024

- At 00:00 UTC, the atmosphere is weakly stable, with CAPE = 0 J/kg, CIN = 0 J/kg, and LI = 1.4°C, indicating limited convective potential. The K-index (27.0) and TTI (53) suggest marginal instability, while precipitable water (16.5 mm) indicates moderate moisture. The freezing level is high (795 hPa), consistent with a relatively warm and stable atmospheric column.
- At 12:00 UTC, a strong destabilization occurs, with CAPE increasing to 374 J/kg and LI dropping to -1.7°C, indicating clearly unstable conditions favorable for convection. The K-index (27.5) and TTI (54) slightly increase, while precipitable water rises to 19.2 mm, supporting moist convection. The freezing level (814 hPa) increases slightly, consistent with enhanced thermal activity.

The day of April 13, 2024

- At 00:00 UTC, the atmosphere shows weak instability, with CAPE = 69 J/kg and a slightly negative CIN of -2 J/kg, indicating limited but existing convective readiness. The LI (2.4°C) reflects a generally stable stratification, while the K-index (28.7) and TTI (47) suggest marginal conditions with no organized convection expected. The precipitable water is relatively high (26.9 mm), indicating a moist atmosphere despite weak instability. The freezing level (756 hPa) indicates a moderately warm vertical thermal structure.
- At 12:00 UTC, the atmosphere remains generally stable to weakly unstable, with CAPE increasing to 158 J/kg, showing a slight improvement in convective potential. However, the LI (-0.5°C) indicates a near-neutral state, while the K-index decreases to 23.2, suggesting reduced convective favorability compared to the morning. The TTI (52) increases slightly, but overall conditions remain weakly supportive of convection. The precipitable water decreases to 17.6 mm, indicating a drying of the atmospheric column, which limits convective development despite the increase in CAPE. The freezing level rises to 789 hPa, consistent with slight warming of the atmospheric profile.

The day of April 14, 2024

- At 00:00 UTC, the atmosphere is weakly unstable, with CAPE = 21 J/kg, CIN = -91 J/kg, and a near-neutral LI of 0.2°C, indicating limited but present convective potential. The K-index (27.9) and TTI (51) suggest marginal instability without organized convection. The precipitable water (21.3 mm) indicates sufficient moisture, while the freezing level (759 hPa) reflects a moderately warm vertical structure.
- At 12:00 UTC, a strong destabilization occurs, with CAPE increasing sharply to 1183 J/kg and LI dropping to -5.3°C, indicating a strongly unstable atmosphere highly favorable for convection. The K-index (25.4) and TTI (49) remain moderate but are overshadowed by the strong thermodynamic instability. The precipitable water (20.9 mm) remains sufficient to sustain deep convection, while the freezing level decreases to 733 hPa, consistent with enhanced vertical development potential.

III.4.3. Comparative analysis of atmospheric stability between both regions

During the period (12–14 April 2026) Laghouat and Ouargla, both regions show a clear diurnal destabilization from 00:00 to 12:00 UTC, but with different intensities.

Laghouat remains generally stable to weakly unstable, with low CAPE values and mostly positive LI, indicating limited convective potential.

Ouargla, in contrast, shows a much stronger instability, with CAPE reaching up to 1183 J/kg and strongly negative LI, especially during daytime heating.Moisture is sufficient in both regions, but Ouargla combines it with a stronger thermodynamic response, including lower freezing levels during unstable periods, favoring deeper convection. Overall, Ouargla is more sensitive to diurnal heating and significantly more conducive to convective development than Laghouat. CAPE and LI are the most sensitive and reliable indices for detecting atmospheric instability in both regions. The observed atmospheric conditions show a clear link with a potential convective (thunderstorm) event, especially during daytime when CAPE increases and LI becomes neutral to negative. These conditions indicate an environment favorable to the development of convective rainfall and thunderstorms, particularly in Ouargla where instability is stronger. However, in Laghouat, the weaker instability suggests a limited convective rainfall potential.

III.5. Conclusion

At 00 UTC, the atmosphere is generally stable to weakly unstable, with low CAPE values (0–69 J/kg) and positive Lifted Index values (up to +2.4 °C), indicating limited potential for deep convection and no significant thunderstorm activity. However, at 12 UTC, a strong destabilization is evident, especially during the most active situation, where CAPE rises sharply (up to 1183 J/kg) and the Lifted Index becomes strongly negative (down to −5.3 °C). The disappearance of CIN and the relatively high moisture content (precipitable water around 20–26 mm) confirm the establishment of a favorable environment for convective development. The sensitivity of the indices, CAPE and LI appear to be the most reliable indicators for this type of convective event in arid environments. CAPE effectively captures the available buoyant energy, while LI provides a direct measure of atmospheric instability in the mid-troposphere. KI and TTI also show moderate sensitivity to moisture and temperature structure, but they are less discriminative in strongly dry environments. CIN, on the other hand, plays a key role in controlling the initiation of convection; its disappearance at 12 UTC coincides with the onset of favorable conditions for convective development.

These results clearly show that the studied rainy–thunderstorm event is associated with a pronounced daytime destabilization of the atmosphere, leading to conditions supportive of convective activity and possible thunderstorm formation during the afternoon period.

GENERAL CONCLUSION

General conclusion

This study investigated the atmospheric conditions associated with the observed rainy–thunderstorm event over the arid regions of Laghouat and Ouargla during 12, 13, and 14 April 2024, using ERA5 reanalysis data provided by the ECMWF. The adopted methodology, based on thermodynamic instability indices derived from vertical profiles (SkewT logP), proved to be well-suited for diagnosing convective potential in data-sparse arid environments.

During the nighttime (00 UTC), the atmosphere is generally stable to weakly unstable, with low CAPE values and positive or near-zero Lifted Index, indicating limited convective activity. In contrast, the 12 UTC soundings systematically reveal a marked destabilization, characterized by increasing CAPE, decreasing or strongly negative LI, and a reduction or complete disappearance of CIN, especially during the most active day of the event.

The sensitivity of the indices, CAPE and LI appear to be the most reliable indicators for this type of convective event in arid environments. KI and TTI also show moderate sensitivity to moisture . CIN, on the other hand, plays a key role in controlling the initiation of convection;.

In the context of arid and semi-arid climates, such as the study area, the low background humidity and strong surface heating enhance the importance of daytime thermodynamic forcing.

Convective events are therefore highly dependent on short-lived but intense destabilization phases. This explains the strong contrast observed between 00 UTC and 12 UTC conditions.

Finally, this study highlights the effectiveness of combining ERA5 reanalysis data with instability indices for diagnosing convective environments in arid regions

As a perspective, future work could use higher-resolution models, satellite observations, and simple machine learning methods to better predict thunderstorm events in desert regions. A longer climatological study would also help define more reliable threshold values for key indices such as CAPE and LI in arid areas like southern Algeria.

BIBLIOGRAPHIC REFERENCES

Bibliographic References

[1] Lalande, J.-M. (2012). Caractérisation des vents dans la moyenne atmosphère et basse thermosphère à partir d'observations d'ondes infrasonores (Thèse de doctorat), École Centrale de Lyon.

[2] World Meteorological Organization (WMO). (2008). Guide des instruments et des méthodes d'observation météorologiques (WMO No. 8). Geneva: World Meteorological Organization.

[3] Rochas, M., & Lagadec, M. (1994). La radiosonde à 65 ans. La Météorologie, No. 6

[4] National Weather Service (NWS). (n. d.).Global Distribution of Radiosonde Launch Sites National Oceanic and Atmospheric Administration (NOAA) . https://www.weather.gov

[5] Gaume, J.-L. (2002). L'observation in situ en altitude. La Météorologie, No. 39.

[6] Vaisala. (2011). Radiosonde Vaisala RS92-SGP [Brochure technique]. Site de l'Instrumentarium de Recherche Atmosphérique par Télédétection (SIRTA). Récupéré de http://sirta.ipsl.polytechnique.fr

[7] Leroy, M., & Grégoire, P. (2005). Mesures en météorologie. Météo-France, Direction de la Météorologie National.

[8] rsbach, H., Bell, B., Berrisford, P., Hirahara, S., Horányi, A., Muñoz-Sabater, J., et al. (2020). The ERA5 global reanalysis. Quarterly Journal of the Royal Meteorological Society, 146(730), 1999-2049. https://doi.org/10.1002/qj.3803

[9] Wallace, J. M., & Hobbs, P. V. (2006). Atmospheric science: An introductory Survey Academic Press.

[10] Stull, R. B. (2015). Practical Meteorology: An Algebra-based Survey of Atmospheric Science: University of British Columbia.

[11] Barry, R. G., & Carleton, A. M. (2001). Atmosphere, Weather and Climate (8th ed). Routledge.

[12] Cairo, F. (2011).Atmospheric Thermodynamics. In Thermodynamics – Interaction Studies-Solids, Liquids and Gases .InTech. https://doi.org/10.5772/19429

[13] Saïdi, H. (2011). Cours de thermodynamique de l'atmosphère. Centre de Publication Universitaire, Manouba, Tunisie.

[14] Thomasse, K. (n.d.). The atmosphere and Skew-T log (p) charts. Avionics West Retrieved from https://www.avionicswest.com/

[15] Torlaschi, E., & Monteiro, E. (s. d.). Introduction à la thermodynamique de l'atmosphère : Notes de cours PHY4501.

[16] Hache, E. (2014). Apport de la bande de Chappuis pour la mesure de l’ozone depuis un satellite géostationnaire pour la surveillance de la qualité de l’air (Thèse de doctorat, Université Toulouse III.

[17] Illinois State Water Survey (.n.d). Review of thermodynamic parameters: LCL, CCL, LFC, and EL. University of Illinois at Urbana-Champaign.

[18] Newell, A. & Galang, B. (n.d.).Skew-T Log-P Diagram |Overview & Lifting Condensation Level. Lesson from the course "Earth Science 104: Intro to Meteorology", Study.com

[19] EUMeTrain. (n.d.). "Stability Indices," in Manual of Synoptic Satellite Meteorology (SATMANU), Finnish Meteorological Institute (FMI) and ZAMG, [Online]. Available:https://rammb.cira.colostate.edu/wmovl/vrl/tutorials/satmanu-eumetsat/satmanu/basic/convection/Parameters.htm